JGR Atmospheres

RESEARCH ARTICLE
10.1029/2022JD037953

Future Projections of EURO-CORDEX Raw and Bias-Corrected Daily Maximum Wind Speeds Over Scandinavia

Clio Michel[1,2] **and Asgeir Sorteberg**[1,2]

[1]Geophysical Institute, University of Bergen, Bergen, Norway, [2]Bjerknes Centre for Climate Research, Bergen, Norway

Key Points:

- The variance in the bias of the mean daily maximum wind speed mainly comes from the choice of the regional climate model
- The ensemble mean change by 2071–2100 shows a moderate increase in the mean wind speed over Scandinavian land except the Norwegian coast
- Bias correction modifies the amplitude of the future wind speed changes, not their pattern

Supporting Information:

Supporting Information may be found in the online version of this article.

Correspondence to:

C. Michel,
Clio.Michel@uib.no

Citation:

Michel, C., & Sorteberg, A. (2023). Future projections of EURO-CORDEX raw and bias-corrected daily maximum wind speeds over Scandinavia. *Journal of Geophysical Research: Atmospheres*, *128*, e2022JD037953. https://doi.org/10.1029/2022JD037953

Received 4 OCT 2022
Accepted 6 FEB 2023

Abstract Twenty historical and future Coordinated Regional Climate Downscaling Experiment ensemble for Europe simulations are bias corrected to investigate the future changes in the daily maximum wind speed over Scandinavia. We use quantile mapping to adjust the wind for the historical period (1985–2014) and quantile delta mapping for two future periods (2041–2070, 2071–2100, RCP8.5) with the 3-km spatial resolution NORA3 hindcast as the reference data set. Decomposing the variance, we find that most of the inter-model spread in the bias and the response to climate change is due to the regional climate model over land and mainly to the general climate model over sea. On average, the mean daily maximum wind speed is projected to increase everywhere except along the western coast of Norway and Denmark. In summer, we see an opposite sign over Sweden and Finland. The Norwegian Sea experiences weaker mean and high wind whereas the Baltic Sea experiences a strengthening. Bias correction influences the amplitude of the response, not the response pattern. Wind speed distributions can have different shapes in the future, with, for example, a flattening of the distribution off the coast of Norway with more frequent weak and very strong winds. Apart from a few locations in Norway, we find an increase in the number of days in the local highest historical wind category. Overall, summer exhibits opposite signals compared to the three other seasons. At country scale, the sign of the change in the mean and 98th percentile varies greatly depending on the region and among the simulations, especially for Norway.

Plain Language Summary The Coordinated Regional Climate Downscaling Experiment ensemble for Europe consists in running regional climate models (RCMs) to improve the spatial resolution and climate simulation of global climate models outputs. In the present study, we use 20 of these simulations, named downscalings, to investigate future changes in the daily maximum wind speed over Scandinavia. As models are not perfect, they present some biases that we correct using quantile mapping, a method adjusting the whole wind speed distribution toward a reference distribution. The reference chosen is the Norwegian hindcast NORA3 that has a 3-km spatial resolution. We show the added value of downscaling and that the bias pattern over land is mainly driven by the RCM. However, the bias correction does not modify the patterns of the future changes in wind speed. On average, the mean daily maximum wind speed will increase in Sweden, Finland, and southeastern Norway whereas it will decrease over Denmark and the Norwegian coast. Although the changes are small, more than 80% of the countries' area has the same response sign, except Norway. Over most of Scandinavia, the number of days within the category of largest historical local wind increases in the future. As in previous studies, we find large model uncertainties in the future projections.

1. Introduction

The present study investigates near-surface winds over Scandinavia in historical and future climates using the multi-model Coordinated Regional Climate Downscaling Experiment (CORDEX) ensemble for Europe (EURO-CORDEX; Jacob et al., 2014). While temperature and precipitation are the two most studied variables in the context of climate change, wind close to the surface, despite its potential for leading to large damages when strong, is less frequently addressed. The main reasons for this are the wind's inaccurate representation in coarse resolution climate models and even in some higher resolution models (e.g., Hewson & Neu, 2015; Kunz et al., 2010; Laurila et al., 2020; Li et al., 2019; McInnes et al., 2011) and the lack of high-quality gridded wind reference data set. Therefore, in order to reliably estimate any change in wind, higher resolution simulations of regional climate models (RCMs) are needed along with bias correction to adjust their outputs toward a reference data set. Here, we make use of a multi-model ensemble of EURO-CORDEX high resolution downscal-

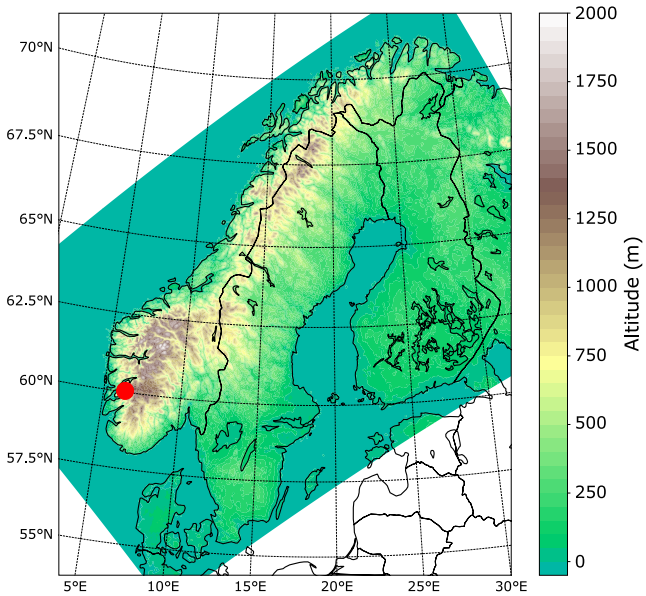

Figure 1. Topography of Scandinavia used in the NORA3 hindcast over the domain of the study. The red point shows the location used for Figure 2.

ing simulations corrected using a very high resolution hindcast simulation (NORA3 by Haakenstad et al., 2021) as reference to examine the wind over Scandinavia (Figure 1) in historical and future periods.

Wind can arise from various meteorological phenomena (see e.g., Markowski & Richardson, 2010). A large pressure gradient, as found around cyclones, is associated with intense geostrophic wind at the surface. In extratropical cyclones, there can also be strong winds along the fronts. Temperature gradients may also trigger wind, such as land-sea and mountain-valley breezes and katabatic/anabatic winds. At smaller horizontal scale, updraft (inflow) and downdraft (outflow) under thunderstorms can lead to very intense winds. Local effects such as channeling of the wind in valleys or fjords can accelerate it. At the spatial resolution of the regional models we use, larger scale winds associated with cyclones, mesoscale topographic effects, and some mesoscale thermally driven winds are resolved, while local scale wind phenomena remain unresolved.

Regional climate simulations showed that, over Scandinavia, the 2-m temperature will change from about 3°C in the south to more than 6°C in the north with a larger warming in winter than summer (see Figure 1 in Christensen et al. (2022)). Although Christensen et al. (2022) showed that the relative changes in the mean wind speed and 10-year return wind do not seem to directly depend on the mean temperature change, global warming can affect the near-surface wind in various ways. Changes in the large-scale circulation can alter the mean jet position, driving windstorms more frequently in certain areas, as well as the number and intensity of extratropical cyclones (Seneviratne et al., 2021). However, the projections depend on the model, emission scenario, and whether internal variability of the climate system is well sampled. For example, a subset of 10 members of the large-ensemble of the Community Earth System Model (CESM-LE), run under the Representative Concentration Pathway 8.5 (RCP8.5), show more (less) cyclones in the Norwegian Sea and over northern (southern) Scandinavia from October to March during the last decade of the century (Dolores-Tesillos et al., 2022). In contrast, using nine global climate models (GCMs) of the latest generation, part of the Coupled Model Intercomparison Project Phase 6 (CMIP6), Priestley and Catto (2022) found more (less) frequent cyclones in southern (northern) Scandinavia in winter by the end of the century under all Shared Socioeconomic Pathways (SSP). Despite these opposite although not statistically significant results, both Dolores-Tesillos et al. (2022) and Priestley and Catto (2022) agree on stronger and wider wind footprints of cyclones at 850 hPa at the time of the cyclone's maximum intensity.

At smaller scales, decreases (increases) in the atmospheric static stability or surface roughness can strengthen (weaken) the wind (e.g., Desai et al., 2009). Desai et al. (2009) found increased wind speeds with time in summer over Lake Superior, one of the Great Lakes in North America, that they linked to the lake water warming faster than the air above, destabilizing the atmosphere thus increasing the winds. In winter, the lake is warmer than the surrounding land, which creates large horizontal temperature and pressure gradients that can be associated with stronger winds (Rouse, 2009). Seo and Yang (2013) and Mioduszewski et al. (2018) showed that increased winds happen in regions where surface warming is large and sea ice retreating attributing it to decreased stability and lower roughness of open water compared to sea ice. In Norway, mountains are very present (Figure 1) and the flow around them can be modified, either by a change in the large-scale atmospheric circulation (direction or intensity) or by changes in stability. If the air becomes more stable, an air parcel will be less likely to go up the mountain than around it (Markowski & Richardson, 2010). Moreover, if the air passing over mountain tops is more (less) stable, the wind will be accelerated more (less) (Coppin et al., 1994).

There is a high uncertainty in the projections of the future wind speed close to the surface. Using a percentile or return values of wind gust, daily maximum wind speed, or mean wind speed, many studies found an increase in the extreme wind in downscaled simulations (Donat et al., 2011; Haugen & Iversen, 2008; Nikulin et al., 2011; Outten & Sobolowski, 2021; Pryor et al., 2012; Schwierz et al., 2010). Downscaling the Norwegian GCM (NorESM) to a 1 km × 1 km spatial grid over a small region of southwestern Norway for 8 years in the 1990s and 2050s, Xu (2019) found that extreme winds were not significantly changing in winter but that they

increased in summer in two specific locations. However, as mentioned above, it is difficult to get an idea of the possible future changes because of the large uncertainty due to both the global and regional models (Christensen et al., 2022; Nikulin et al., 2011; Outten & Esau, 2013; Outten & Sobolowski, 2021; Schwierz et al., 2010), the emission scenario, and the internal variability. Pryor et al. (2012) showed that downscaling two simulations from one GCM can lead to very different results, thus highlighting the importance of internal variability in the future wind speed change. Using three downscaled simulations, Schwierz et al. (2010) found that the GCM driving the regional model has the largest impact on the mean and 98th percentile of the wind gust and their future changes (see their Figures 6 and 7). An additional source of uncertainty is the sensitivity to the distribution (e.g., generalized extreme value, Pareto, or Weibull) chosen to obtain the return values (see e.g., Figure 3 of Lawrence (2020)).

Despite their increase in resolution and improvement, models still struggle to well simulate the wind close to the surface (Laurila et al., 2020). The roughness length of sea and land affects the wind speed and needs to be taken into account by models. Therefore, in order to counteract the coarse orography, low-resolution models use a high roughness or a sub-grid orographic drag parameterization scheme over mountainous regions but this unrealistically slows down the near-surface wind. Laurila et al. (2020) recently showed that this issue appears in the latest ERA5 reanalysis with very weak winds over the Alps, Pyrenees, and the Norwegian mountains. The main solution to this problem is the use of very-high resolution models that have a realistic orography and surface roughness and are therefore able to resolve the small-scale processes associated with it (e.g., Cheynet et al., 2020). Another solution is to adjust the coarse model output toward a reference data set so that it becomes more realistic (e.g., Moemken et al., 2018).

In order to make more accurate regional impact assessments, one needs to rectify the bias of the models outputs. The simplest statistical bias correction method is to adjust the mean values toward the mean of a reference data set. Other methods correct higher statistical moments of the distribution, such as the standard deviation, skewness, and kurtosis to also adjust the data variability (see e.g., Li et al., 2019, for a short review). Some methods such as the quantile mapping correct the whole distribution but are not exempt of issues especially if the resolution of the simulation is much coarser than the resolution of the reference data set (see e.g., Maraun, 2013, for precipitation). Bias correction methods may also want to preserve trends and the climate change signal (Amengual et al., 2012; Cannon et al., 2015; Hempel et al., 2013; Lange, 2019). As bias correction is applied to finite time series at individual grid points, the spatial and temporal consistency is not guaranteed. Important assumptions are that the future climate has the same variability as the reference data set, which may not be true (Chen et al., 2020), and the same bias as the historical climate. Overall, one needs to know the deficiencies of the bias correction method chosen (François et al., 2020).

As wind is represented by a vector in climate models, previous studies have corrected the wind direction to drive wave models (Hemer et al., 2012; Jing-Jing et al., 2014), its two horizontal components using a multivariate bias correction method (Li et al., 2020), or its length, the wind speed (Barstad et al., 2012; Li et al., 2019; Tobin et al., 2015). However, to perform bias correction, one needs a reliable reference data set such as observations or a gridded data set. Several attempts have been made to grid wind observations using interpolation methods (e.g., Abatzoglou (2013), Brinckmann et al. (2016), and the E-OBS data set by Cornes et al. (2018)) but the task is not straightforward as near-surface wind observations are very much affected by local conditions. In addition to observation uncertainty, such as change in measurement technique and station location (Haakenstad et al., 2021), Brinckmann et al. (2016) found a lack of accuracy in exposed/high-altitude areas. The absence of reliable gridded data set is the main reason why most studies use the raw output of the RCMs to study the mean and extreme wind over Scandinavia (see e.g., the two recent studies by Outten and Sobolowski (2021) and Christensen et al. (2022)).

In the present study, we will make use of a 3-km spatial resolution hindcast (Haakenstad et al., 2021), that has been proved to be comparable to observations in Norway (Cheynet et al., 2022; Haakenstad et al., 2021; Solbrekke et al., 2021; for offshore wind validation), to bias correct the wind speed simulated by the EURO-CORDEX models over Scandinavia (Figure 1). This, to our knowledge, has not been done before. We will then examine both raw and bias corrected daily maximum wind speed hence showing the impact of bias correction on the projected changes in wind.

Table 1
Matrix of the 20 Historical and Future (RCP8.5) Coordinated Regional Climate Downscaling Experiment Ensemble for Europe (EURO-CORDEX) Simulations Used in This Study

RCM/GCM	CNRM-CM5	EC-EARTH	IPSL-CM5A-MR	MPI-ESM-LR	NorESM1-M
KNMI-RACMO22E	r1, v2	r12, v1	r1, v1	r1, v1	r1,v1
DMI-HIRHAM5	r1, v2	r12, v1	r1, v1	r1,v1	r1, v1
IPSL-WRF381P	r1, v2	r12, v1	r1, v1	r1, v1	r1,v1
SMHI-RCA4	r1, v1	r12, v1	r1, v1	r1, v1a	r1,v1

Note. The letter "r" denotes the realization and the letter "v" the version of the simulation. KNMI stands for the Royal Dutch Meteorological Institute, DMI for the Danish Meteorological Institute, IPSL for the Pierre Simon Laplace Institute, and SMHI for the Swedish Meteorological and Hydrological Institute.

2. Data and Methods

2.1. EURO-CORDEX Simulations

We here examine the daily maximum near-surface wind speed of the CORDEX downscaling simulations over the European domain (EUR-11) which have a spatial resolution of ∼12.5 km (Jacob et al., 2014). Twenty combinations of five GCMs downscaled with four different RCMs have been chosen as listed in Table 1. We use the historical experiment and the RCP8.5 experiment for the future. We focus on three 30-year periods: a historical period covering 1985–2014 by merging the historical (1985–2005) and RCP8.5 (2006–2014) experiments, a near-future period covering 2041–2070, and a far-future period covering 2071–2100 under RCP8.5.

The daily maximum wind speeds from CMIP5 GCMs downscaled in the EURO-CORDEX exercise are used here to evaluate the advantage of downscaling. Only three GCMs, out of the five listed in Table 1, provided the appropriate variable (sfcWindmax): CNRM-CM5, IPSL-CM5A-MR, and MPI-ESM-LR.

Note that the daily maximum wind speed is computed using all model timesteps available by the RCMs and GCMs.

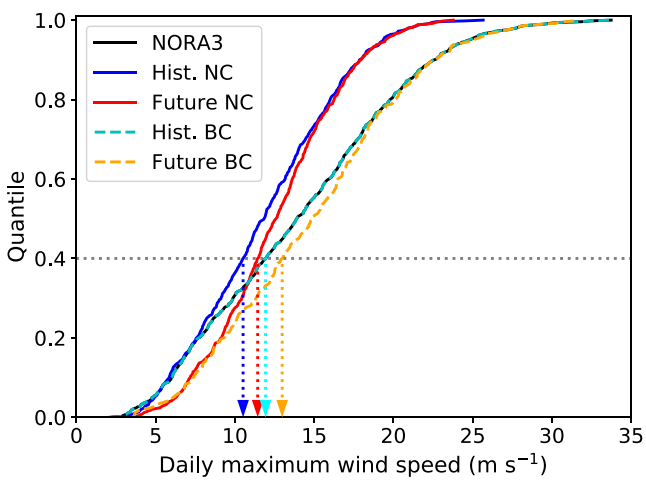

Figure 2. Empirical cumulative distribution functions (ECDFs) illustrating the bias correction process for one grid point (displayed in Figure 1) and the month of January. The black line represents the ECDF for the reference NORA3. The solid blue and red lines represent the non-corrected (NC) ECDFs for the historical and far future experiments, respectively, for the model CNRM-CM5 downscaled with RCA4. The dashed cyan and orange lines represent the bias corrected (BC) ECDFs for the historical and far future experiments, respectively. The dotted gray line highlights the 40th percentile and the arrows point toward the associated wind speed values.

2.2. The NORA3 Hindcast

The Norwegian Meteorological Institute has created a high-resolution hindcast, named NORA3 (3-km Norwegian reanalysis), using the latest reanalysis from the European Centre for Medium-Range Weather Forecasts, ERA5 (Hersbach et al., 2020), as forcing to the non-hydrostatic numerical weather prediction model HARMONIE-AROME (Haakenstad et al., 2021). The hindcast is the aggregation of 9-hr forecasts run every 6 hr. Forecast lead times from 4 to 9 hr are used, discarding the first forecast with a 3-hr lead time to allow for some spin-up time. We end up with an hourly product on a 3 km × 3 km spatial grid covering Scandinavia (Figure 1). NORA3 is freely available at https://thredds.met.no/thredds/catalog/nora3/catalog.html (last access: 28 July 2022). NORA3 has demonstrated very good skills in simulating the wind speed compared to observations (Haakenstad et al., 2021; Solbrekke et al., 2021) and will be used as reference data set to bias correct the EURO-CORDEX simulated daily maximum wind speed. We use the hourly wind speed at 10 m to calculate the daily maximum wind speed to approximately match the variable from the CORDEX simulations computed using more timesteps, for the same period 1985–2014. In their Figures 3b and 3c, Pinto et al. (2007) showed that using a lower sampling (every 6 hr) instead of the model timesteps leads to an underestimation of the daily maximum wind speed, as expected. Therefore, the differences between the EURO-CORDEX simulations and NORA3 do not only arise from the models but also from the different temporal sampling to calculate the daily maximum wind speed.

2.3. Bias Correction

First, EURO-CORDEX simulations are regridded on the NORA3 grid, for a reduced overlapping domain (Figure 1), using the nearest-neighbor method to avoid any issue with averaging/interpolating, hence keeping the high and low extremes as simulated by the RCMs. Second, the bias correction is performed using the quantile mapping method for the present period (1985–2014) and using the quantile delta mapping for the two future periods (see e.g., Cannon et al., 2015; Li et al., 2019; Tong et al., 2021). We correct each calendar month over the 30 years separately (e.g., 30 January months at a time) in order to preserve the seasonal cycle and reduce the seasonal mean bias.

The quantile mapping method consists in adjusting the cumulative distribution function (CDF) (or quantile functions) of the simulated wind toward the CDF of the reference data set, this operation being performed at each grid point separately. The CDFs are built using percentiles every 0.2%. The adjustment of the CDF of the historical simulated wind speed $w^r_{m,h}$ can be expressed as follows:

$$w^c_{m,h}(t) = \mathcal{F}^{-1}_{o,h}\left\{\mathcal{F}_{m,h}\left[w^r_{m,h}(t)\right]\right\} \tag{1}$$

where w is the wind speed, $\mathcal{F}$ represents the CDF and $\mathcal{F}^{-1}$ its inverse function, the superscripts c and r refer to the corrected and raw wind, respectively, the subscript o refers to NORA3, m to the CORDEX simulations, and h to the historical period. The term within accolades gives the quantile (between 0 and 1) associated with the simulated wind speed $w^r_{m,h}(t)$ and the inverse CDF $\mathcal{F}^{-1}_{o,h}$ gives the NORA3 wind speed associated with this quantile.

For the future periods, we use the quantile delta mapping method as described in Cannon et al. (2015). First, we get the quantile ($\tau_{m,f}(t)$, between 0 and 1) associated with the simulated wind speed in the future period $w^r_{m,f}(t)$.

$$\tau_{m,f}(t) = \mathcal{F}_{m,f}\left[w^r_{m,f}(t)\right] \tag{2}$$

Second, we take the ratio between the simulated future wind speed $w^r_{m,f}(t)$ and the simulated historical wind speed associated with the quantile $\tau_{m,f}(t)$:

$$\Delta_m(t) = \frac{w^r_{m,f}(t)}{\mathcal{F}^{-1}_{m,h}\left[\tau_{m,f}(t)\right]} \tag{3}$$

Third, the adjusted wind speed is the observed/reference historical wind speed associated with the quantile $\tau_{m,f}(t)$ multiplied by the simulated ratio between the historical and future periods. Since we choose to conserve the relative change, we have to multiply by $\Delta_m(t)$ and not add it (as one would do in order to conserve the absolute change). We here choose to conserve the relative change as for parameters that have meteorologically meaningful zero value as a lower boundary as for wind and precipitation, a multiplicative approach is more robust and more common (Hempel et al., 2013). An additive approach (conservation of the absolute change) would easily lead to unphysical negative values of the wind speed.

$$w^c_{m,f}(t) = \mathcal{F}^{-1}_{o,h}\left[\tau_{m,f}(t)\right]\Delta_m(t) \tag{4}$$

Contrary to Cannon et al. (2015), we do not use sliding time windows centered on the year to be corrected.

An illustration of the bias correction process is given in Figure 2 for one grid point (red dot in Figure 1). The black line shows the empirical CDF (ECDF) for the reference data set NORA3 with daily maximum wind speeds between 2.2 and 33.7 m s^{-1}. Comparing the black and solid blue lines, we see that the original simulation (CNRM-CM5 downscaled with RCA4) clearly shows an underestimation in "strong" wind speeds (curve to the left of the reference). When it is bias corrected, the ECDF of the historical simulation overlaps the reference (see dashed cyan line above the black line). Here, the simulated wind speeds outside the reference range are brought back toward the reference. The original future simulation exhibits increased wind speed compared to the historical period, mainly for the bottom half of the distribution (quantile less than 0.6), with the solid red line to the right of the solid blue line. This response can also be seen in the bias corrected future simulation as shown with the dashed orange line to the right of the historical bias corrected ECDF. One can note that using this quantile delta mapping method, future wind speeds can lie outside the historical range (maximum wind speed of 35.4 m s^{-1} in the future).

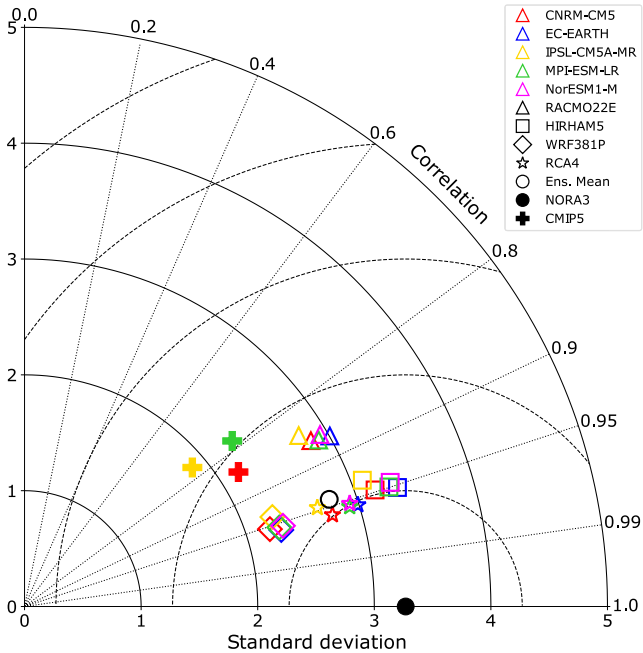

Figure 3. Taylor diagram for the mean daily maximum wind speed for the 20 historical simulations used in the study (colored points) plotted against the reference NORA3 (filled black circle). The ensemble mean of the 20 simulations is shown with an empty black circle. The symbol shape depends on the regional climate model and the color on the global climate model. The standard deviation is expressed in m s^{-1}. The solid circles with origin (0, 0) represent the spatial standard deviation (over the Scandinavian domain) of the mean daily maximum wind speed. The dashed circles with origin (σ_r, 0) show the spatial centered root-mean-square difference, and the dotted lines represent the spatial correlation, following Taylor (2001). The solid and dashed circles are drawn every 1 m s^{-1}.

2.4. Taylor Diagram

To evaluate the mean of the daily maximum wind speed of each downscaling simulations against NORA3, we use a Taylor diagram. Following Equations 1 and 2 of Taylor (2001), we represent the spatial correlation coefficient between the simulated mean and the mean in NORA3 (R), the spatial centered root-mean-square (RMS) difference (E'), and the spatial standard deviation of the mean fields (σ_s for the simulation and σ_r for the reference NORA3). The mean wind speed map of NORA3 is the reference with a spatial standard deviation $\sigma_r \simeq 3.27$ m s^{-1}, $R = 1$, and $E' = 0$. As shown in Taylor (2001), $R = \cos\phi$ where R is the correlation and ϕ the angle between the x-axis and the correlation, also called azimuth. Therefore, the coordinates for each simulation are $x = R\sigma_s$ and $y = \sqrt{E'^2 - (\sigma_r - x)^2}$.

2.5. Analysis of Variance

As we have a full 5 × 4 matrix of simulations (Table 1), we are able to disentangle the variance due to the GCM, the RCM, and their combination following the method described in Déqué et al. (2007). There are only two dependences in our set of simulations: the dependence on the GCM and the dependence on the RCM, as we use only one scenario (either historical or future) and one member for each simulation.

The total variance of the full ensemble of simulations is expressed as:

$$V = \frac{1}{NG}\sum_{g=1}^{NG}\frac{1}{NR}\sum_{r=1}^{NR}(x_{gr} - x_{GR})^2 \tag{5}$$

where g refers to the GCM dimension with $NG = 5$ different GCMs and r refers to the RCM dimension with $NR = 4$ different RCMs. x_{gr} is one individual map for GCM g and RCM r. x_{GR} is the mean over all GCMs and RCMs or in other words the ensemble mean. The total variance can be decomposed as follows:

$$V = G + R + RG \tag{6}$$

where G is the variance attributed to the GCM, R the variance attributed to the RCM, and RG is the variance attributed to the combination of the GCM and RCM. They are respectively defined as follows:

$$G = \frac{1}{NG}\sum_{g=1}^{NG}(x_{gR} - x_{GR})^2 \tag{7}$$

$$R = \frac{1}{NR}\sum_{r=1}^{NR}(x_{Gr} - x_{GR})^2 \tag{8}$$

$$RG = \frac{1}{NG}\sum_{g=1}^{NG}\frac{1}{NR}\sum_{r=1}^{NR}(x_{gr} - x_{gR} - x_{Gr} + x_{GR})^2 \tag{9}$$

where x_{gR} is the mean over all RCMs for GCM g and x_{Gr} is the mean over all GCMs for RCM r. A residual can be calculated to check that Equation 5 is really the sum of Equations 7–9:

$$res = V - (G + R + RG) \tag{10}$$

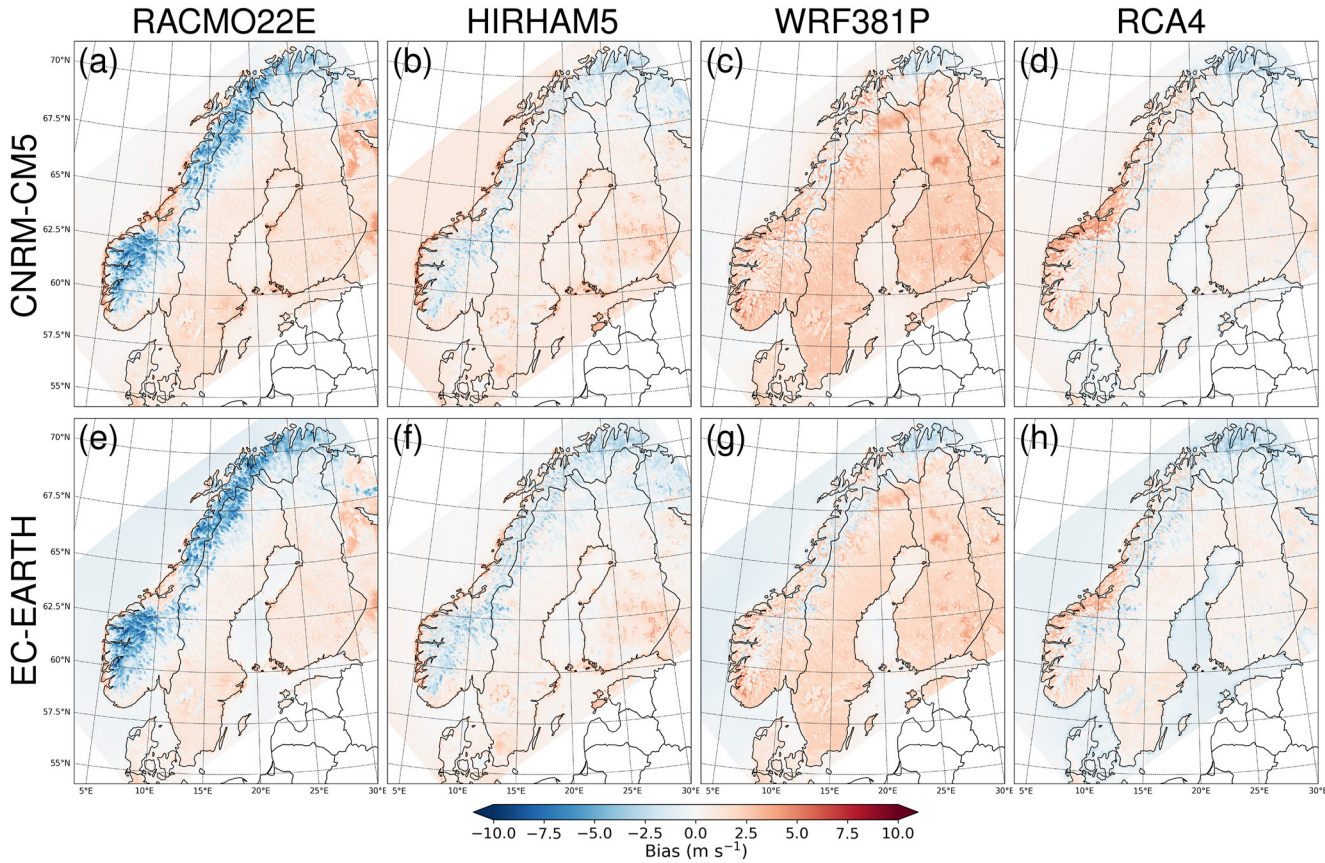

Figure 4. Difference in the mean daily maximum wind speed (m s^{-1}) between the simulations and NORA3 for the historical period 1985–2014. Panels (a–d) are associated with four downscalings of the GCM CNRM-CM5 and panels (e-h) with downscalings of the GCM EC-EARTH. The rest of the simulations are shown in Figure S1 in Supporting Information S1.

3. Results

3.1. Bias in the Historical Mean

The Taylor diagram (Figure 3) shows that the performance of the simulation of the mean daily maximum wind speed relies mainly on the RCM chosen with smaller influence from the GCM. The points are grouped by RCM (different symbols), the colors indicating the various GCMs. Downscalings with RCM HIRHAM5 have the closest spatial standard deviation to NORA3 (~3.27 m s^{-1}) with spatial correlations between 0.936 and 0.952. On the contrary, the downscalings by RCM WRF381P underestimate the spatial standard deviation the most, by 1 m s^{-1}. The downscalings by RCA4 (star symbol) have an overall low spatial centered RMS difference but tend to underestimate the spatial standard deviation. Downscalings having the weakest correlation and the largest centered RMS difference are from RCM RACMO22E. In every group of points, the GCM IPSL-CM5A-MR (yellow symbols) has the weakest spatial correlation and along with GCM CNRM-CM5 (red symbols), tend to stand out from the other three GCMs because of their lower spatial standard deviations. The crosses symbols for three CMIP5 GCMs downscaled in EURO-CORDEX highlight the added-value of downscaling GCMs in order to better represent the daily maximum wind speed (Figure 3).

As shown in Figure 4 and Figure S1 in Supporting Information S1 and in agreement with the Taylor diagram (Figure 3), the difference (or bias) in the mean daily maximum wind speed between the simulation and NORA3 strongly depends on the RCM used. RCM RACMO22E strongly underestimates the mean wind speed over the mountains while slightly overestimating it over land and along the western Norwegian coast (Figures 4a and 4e). RCM HIRHAM5 (Figures 4b and 4f) exhibits a similar bias to RACMO22E with lower values over land but exhibits a marked positive bias over sea. RCM WRF381P mainly features a positive bias over land (Figures 4c and 4g). Finally, RCM RCA4 exhibits a relatively large positive bias along the Norwegian coast between 62° and 65°N (Figures 4d

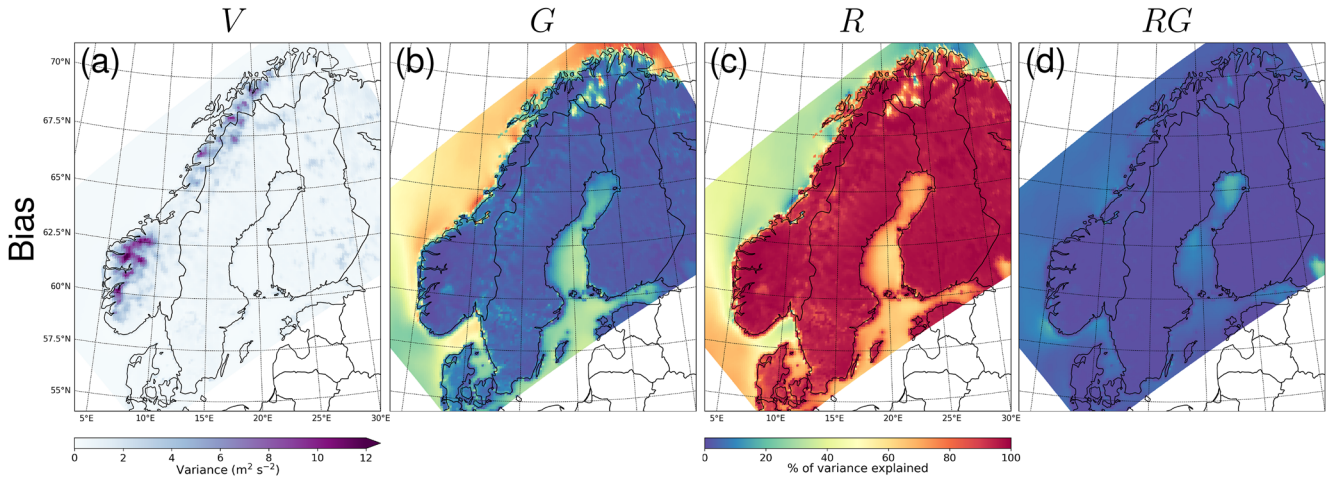

Figure 5. Variance among the 20 simulations and its decomposition for the bias in the mean daily maximum wind speed. (a) Variance *V* of the bias in the mean daily maximum wind speed among the 20 simulations (in m s^{-1}). Percentage of the total variance *V* due to (b) the global climate model (GCM) only (*G*), (c) the regional climate model (RCM) only (*R*), and (d) the combination of the RCM and GCM (*RG*). The sum of *G*, *R*, and *RG* equals 100%.

and 4h). Overall, all RCMs present a positive bias over the low-latitude land, that is southeastern Norway, Sweden, Finland, and Denmark, and a negative bias over the mountains (with different magnitudes) and northern Norway. These differences are probably linked to the still too coarse resolution of the RCMs, not resolving well the complex topography of the region, with a roughness length too high over the mountains and too small over the lower land.

From Figures 4 and 5a, we see that the spread in the bias among the simulations is largest over southwestern Norway and between 65° and 70°N over Norway and part of Sweden because of the various magnitudes of the negative bias over the mountainous areas. A decomposition of the variance of the bias among the simulations (Figures 5b–5d) shows that over land, parts of the North Sea, and the Baltic Sea, the variance is mainly due to the RCM (Figure 5c), while over the Norwegian Sea, Barents Sea, and the strait between Norway and Denmark (Skagerrak), the variance is mainly due to the GCM (Figure 5b). This is in agreement with Vautard et al. (2021) who, although using the daily mean wind speed, found that the bias over land can be mainly attributed to the RCM chosen and only barely to the GCM downscaled (see their Figure 3). For some grid points in the region 68°–70°N/20°–25°E, the variance is not only due to the RCM but also to the GCM and in a smaller extent to the combination RCM-GCM (compare panels b–d in Figure 5). The contribution to the total variance of the combination RCM-GCM is overall very small with some weak "hot" spots (~20%) off the southwestern coast of Norway, where the large-scale atmospheric circulation may interact with the topography, and in the Gulf of Bothnia, where sea ice in winter may play a role. Modifying the set of simulations used, for example, leaving out one GCM or one RCM, can affect the results. The influence of the GCMs considered is quite weak compared to the influence of the RCMs (not shown). For example, leaving out all the four downscalings of the GCM IPSL-CM5A-MR slightly decreases the contribution to the variance from the GCMs but increases the contribution from the RCMs. Leaving out the five downscalings from RACMO22E or WRF381P increases (decreases) the contribution from the GCMs (RCMs) over northern Norway and Sweden, respectively.

3.2. Future Changes in the Raw Mean Winds

The mean daily maximum wind speed in the original EURO-CORDEX simulations for the period 1985–2014 is high over the seas, lakes, and mountains (>9 m s^{-1}), and weak over the low-altitude lands, such as southeastern Norway, Sweden, and Finland (Figure 6a). Denmark, which is more exposed, exhibits higher wind speeds than the norther countries. In winter (Figure 7a), the mean daily maximum wind speed is higher over the sea and Norway while in summer (Figure 8a) it is lower over the seas and Norway but is higher elsewhere.

In the far future experiments, under the RCP8.5 scenario, with 15 out of 20 simulations agreeing on the sign, there is a robust decrease in the mean daily maximum wind speed over the Norwegian Sea and part of the North Sea as well as Norway's coastal region and Denmark (Figure 6b). Over southeastern Norway, Sweden, and Finland, the mean daily maximum wind speed increases slightly but it is not robust. However, over the southern Baltic Sea and the Gulf of Bothnia, there is a robust increase in the mean daily maximum wind speed. This pattern is the same for

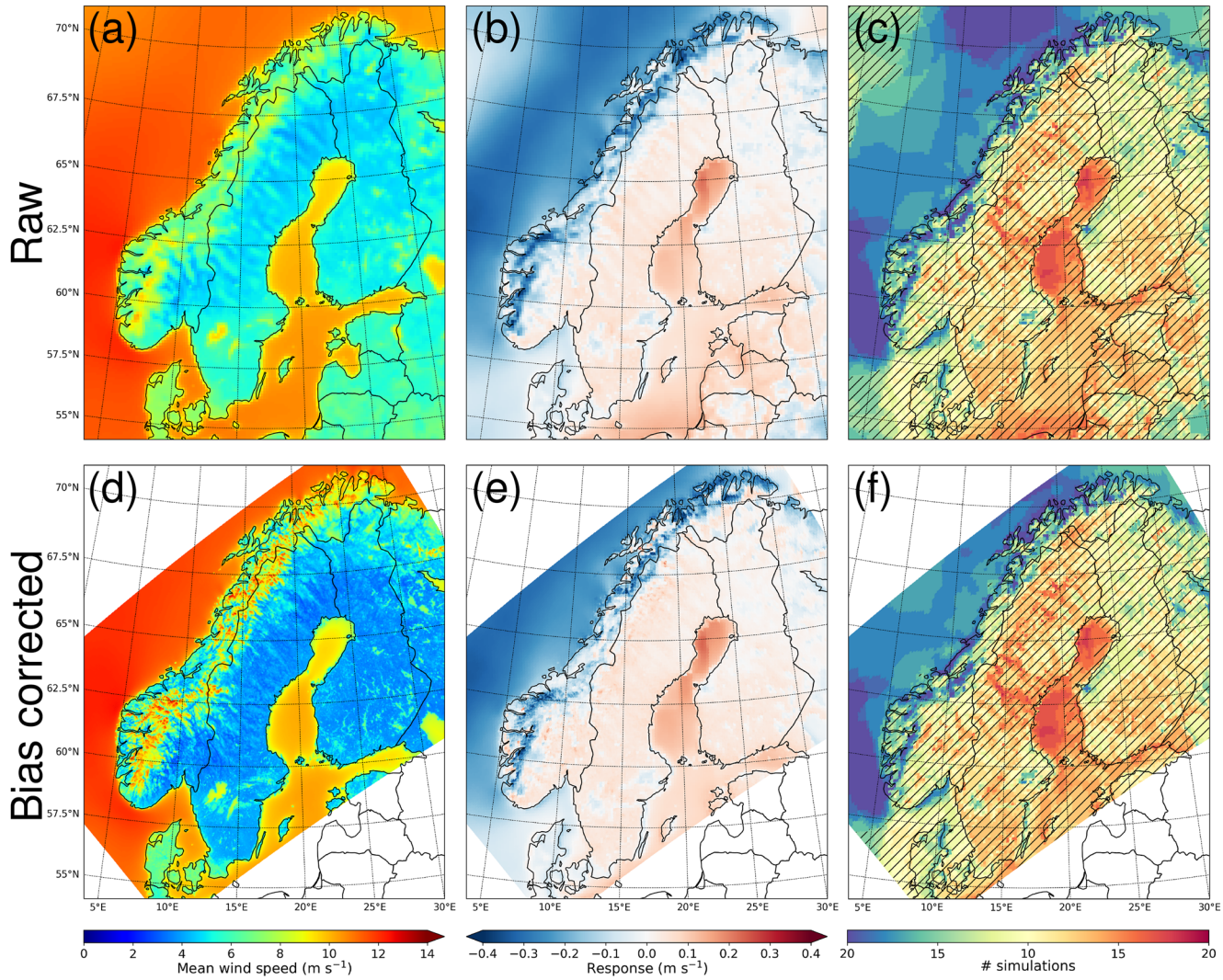

Figure 6. Ensemble mean of the annual mean (top) raw and (bottom) bias-corrected daily maximum wind speed over (a and d) the whole historical period (1985–2014) and (b and e) its change in the far future (2071–2100) relative to the historical period. (c and f) Number of simulations among the 20 that agree on the sign of the change. Green and blue colors denote the same negative sign and orange and red colors the same positive sign. Yellow colors mean that half of the simulations share a negative sign and the other half a positive sign. Hatches highlight areas where less than 80% of the simulations, that is, 16, agree on the sign.

the two future periods with the largest changes in the last 30 years of the century (Figures 6a–6c, Figures S2a–S2c in Supporting Information S1 for the near future), apart from Denmark where the change is less robust in the far future. There seems to be a decrease in the mean daily maximum wind speed over Sweden's lakes, mainly Vänern and Mälaren, contrary to their surroundings but it is not very robust.

In winter, the changes are similar to considering the whole period but larger in magnitude (Figures 7a–7c). In addition, there appears a robust increase in the mean daily maximum wind speed over some parts of southeastern Norway, most of Sweden, and the southern half of Finland. This increase is only robust in the far future period (compare with Figures S3a–S3c). The decreased wind speed on the windward side of the mountains does not systematically lead to lower winds on the lee side. The strengthening east of the mountains may originate from winds coming from other directions than west. In both winter (December-January-February, DJF) and summer (June-July-August, JJA) (Figures 7b and 8b), there is a decrease in the mean daily maximum wind speed over the Norwegian Sea in the future but its location varies from winter to summer as well as from the near future to the far future for DJF (Figures 7b and 8b, Figures S3b and S4b). Over the Baltic Sea and Gulf of Bothnia, the wind speed increases in the future and more particularly in winter. The lack of sea ice in this area in the future winters probably plays a role in this signal (response and trend) as the roughness of the sea is smaller than the

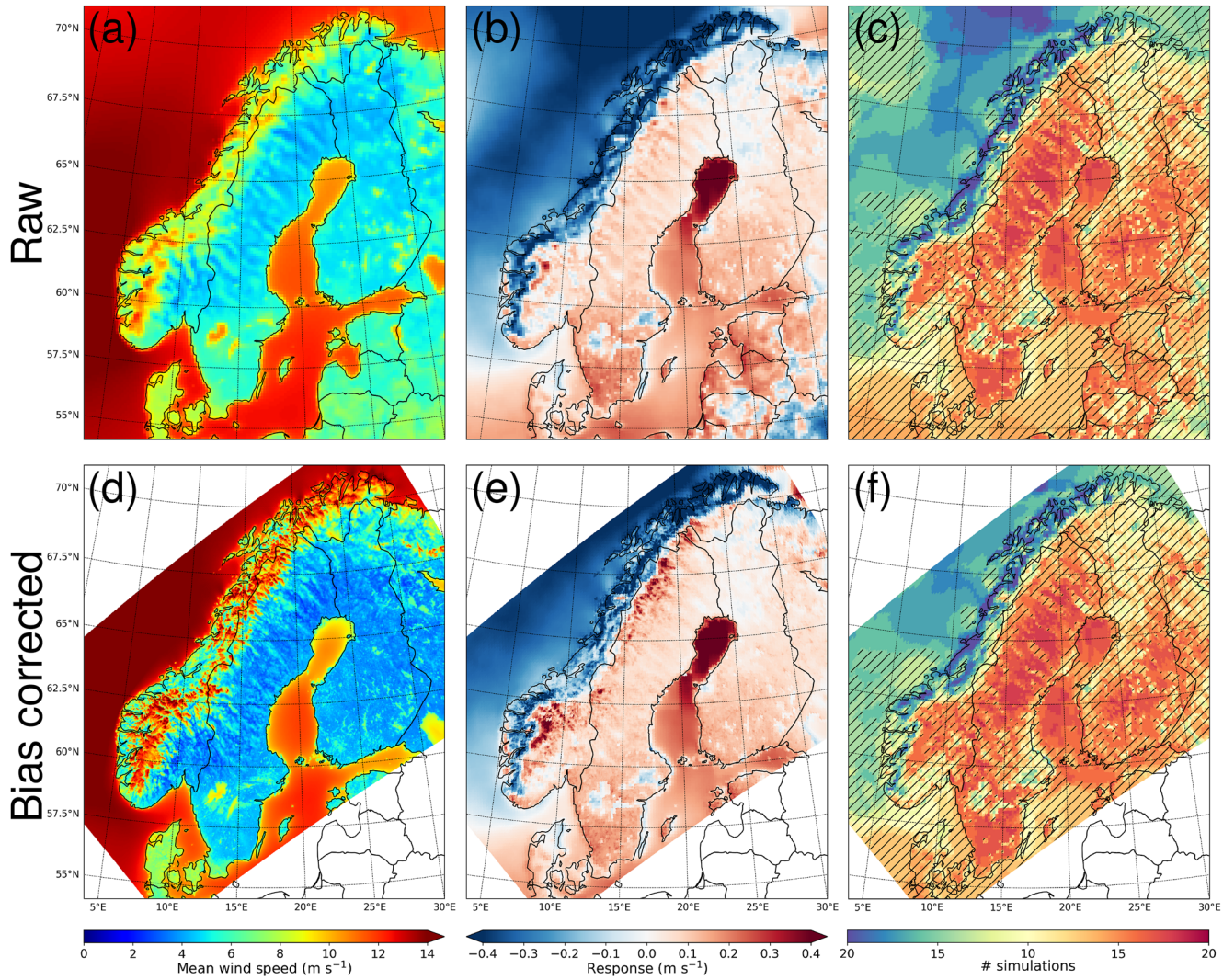

Figure 7. Same as Figure 6 but for winter (December-January-February).

roughness of sea ice (Mioduszewski et al., 2018), which allows a strengthening of the wind close to the surface. In summer, there is a robust decrease in the southern half of Norway and some very local robust increases in the northern half. Opposite to winter, most of Sweden and Finland experience a robust weakening of the mean daily maximum wind speed in summer (Figure 8b). The change is stronger in the far future period, and Denmark along with the three Baltic States experience a robust decrease in mean daily maximum wind speed that did not appear in the near future period (Figure 8b, Figure S4b). Contrary to winter and the whole period, the wind speed slightly increases over Sweden's lakes in summer, which, following Desai et al. (2009), could be associated with the lake warming faster than the overlying air destabilizing the atmospheric boundary layer and accelerating the wind, in conjunction with a shortening in the winter ice season. Another explanation could be a larger land-sea temperature contrast strengthening the sea breeze circulation.

3.3. Future Changes in the Mean and Strong Bias-Corrected Winds

The general patterns of the multi-model ensemble mean change between the uncorrected and the bias-corrected mean daily maximum wind speed are similar but the magnitude of the response can vary (compare the middle column in the top and bottom rows of Figures 6–8 for the far future and Figures S2–S4 in Supporting Information S1 for the near future). Note that as we conserve the relative change during the bias correction, the absolute changes are not expected to be conserved. In winter, over southern Norway and northern Sweden, the changes in the mean daily maximum wind speed become larger compared to the raw data. On the contrary, in summer,

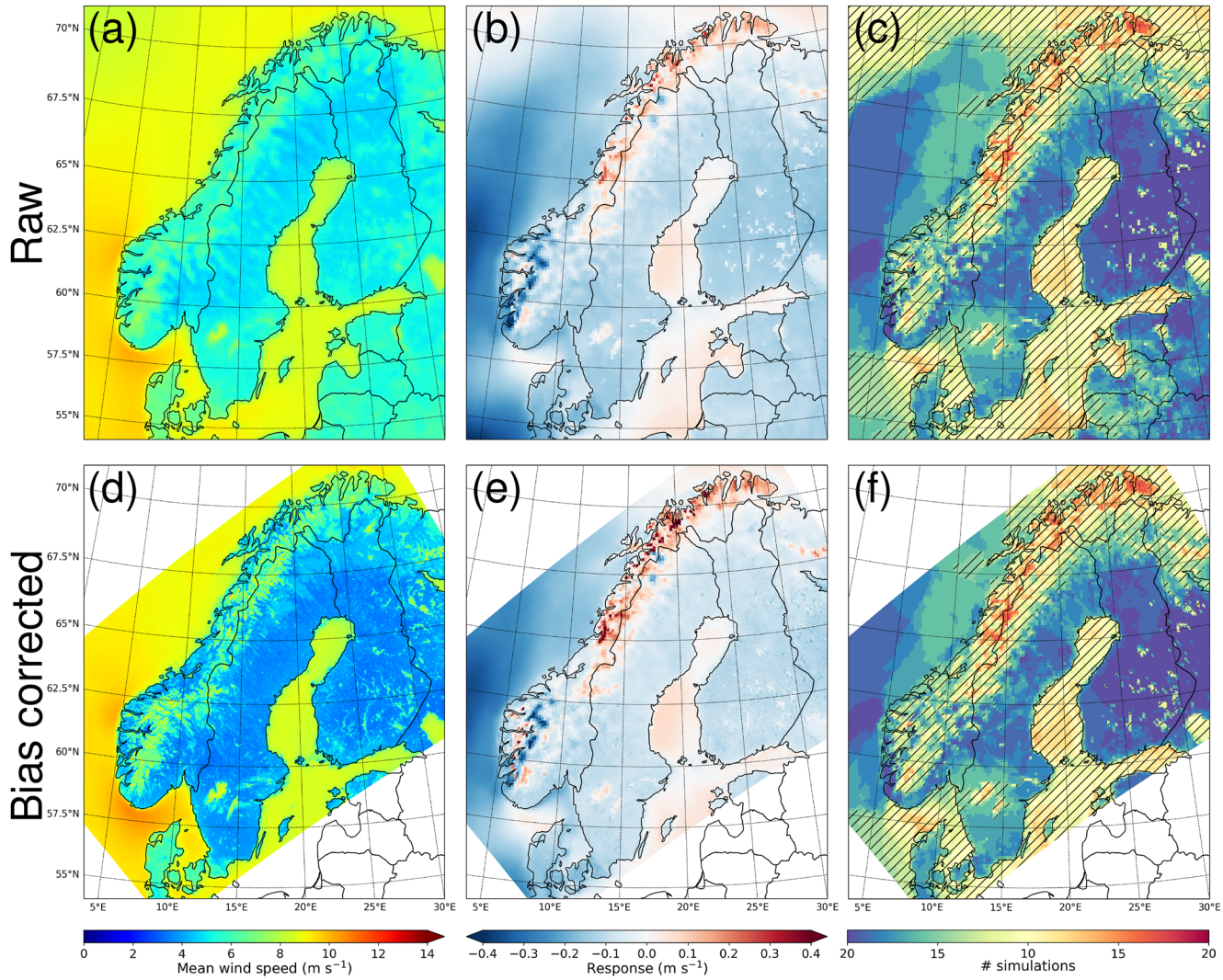

Figure 8. Same as Figure 6 but for summer (June-July-August).

the negative changes over Sweden and Finland become less strong in both future periods. For completeness, Figure S5 displays the changes for spring and autumn. We see that the changes are larger and more robust in spring than autumn with large negative changes over Norway and the Norwegian Sea along with some more modest positive changes over southeastern Norway, Sweden, Finland, and the Baltic Sea.

The analysis of variance shows that the variance, or in other words, the spread among the simulations in the far future change in the mean is largest over northern Norway (Figure 9a). The variance decomposition (Figure 9) shows that the variance over the Norwegian Sea, Denmark, and the Barents Sea is predominantly due to the GCM while over southern Sweden and the Gulf of Bothnia, the change is linked to the RCM, the GCM, and to a lesser extent to the combination RCM/GCM. Over Norway, Sweden, and Finland, the variance in the change is mostly linked to the RCM (see also Figures S6 and S7). Figure S6 displays the changes for each of the 20 simulations of our ensemble highlighting the spread among them. Figure S7 reveals again that independent of the GCM, the RCM is more important in shaping the response of the wind speed. The averages over the four RCMs for each GCM separately (top row) all appear very similar. On the contrary, the averages over the five GCMs for each RCM separately (bottom row) are very different from each other over land (see also Figure S6), the RCM controlling the response pattern. For the near future, the variance in the changes is split more equally among the three sources (GCM, RCM, and their combination) even though the RCM has still the largest share over land and the Baltic Sea and the GCM the largest share over the Norwegian and North seas (Figure S8).

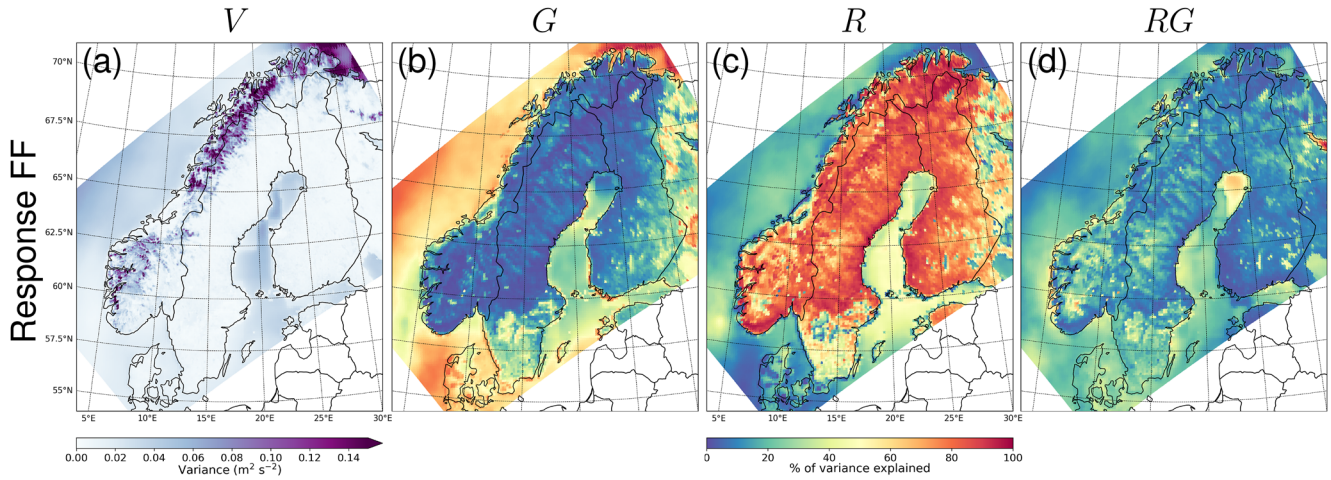

Figure 9. Same as Figure 5 but for the projected changes in the mean of the bias corrected daily maximum wind speed.

The 98th percentile of the daily wind speed is often used as a measure of strong winds (from e.g., the daily maximum wind speed or gust by Schwierz et al. (2010) and Donat et al. (2011)). We here define the 98th percentile using all days in each 30-year period assuming that there is no large temporal trend. It means that about 220 days in 30 years, or ∼6.7 days per year, lie above this percentile. The 98th percentile is largest over the elevated terrain of Norway and northern Sweden (Figure 10a). It is also high over the Norwegian and North seas as well as over the Baltic Sea. Over low-altitude land, the percentile is weaker especially over southeastern Norway, most of Sweden, and Finland. The Norwegian western coast, Denmark, and the big lakes in Sweden experience a relatively high 98th percentile, due to their more exposed location to passing cyclones and low roughness over lakes. The future change in the 98th percentile depends on the area (Figure 10b). It robustly decreases over parts of the Norwegian Sea and Norway, mainly between 62.5° and 65°N and in the far north, whereas it robustly increases over the North and Baltic seas, southern Denmark, southeastern Norway, and most of Sweden and Finland (Figures 10b and 10c). The change in the number of days above the historical 98th percentile has similar sign as the change in the percentile itself but the relative intensity is not the same (Figure 10d). For example, over southern Sweden and Finland, the historical percentile is low (<10 m s^{-1}, Figure 10a) and even a small increase of its value in the future (<0.4 m s^{-1}, Figure 10b) makes that many more days will experience winds above the historical percentile (>60 days over

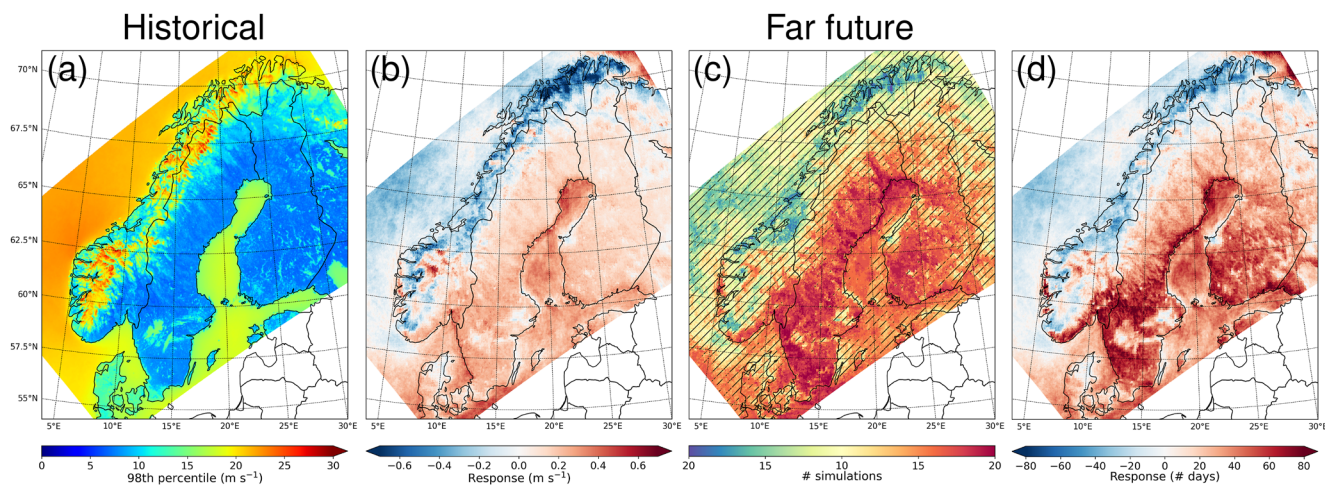

Figure 10. (a) Ensemble mean of the bias-corrected historical 98th percentile of the daily maximum wind speed (in m s^{-1}), (b) of the far future change in the 98th percentile (in m s^{-1}), and (d) of the far future change in the number of days exceeding the historical 98th percentile. (c) Number of simulations among the 20 agreeing on the sign of the change. Green and blue colors denote the same negative sign and orange and red colors the same positive sign. Yellow colors mean that half of the simulations share a negative sign and the other half a positive sign. Hatches highlight areas where less than 80% of the simulations, that is, 16, agree on the sign.

Table 2
Description of the Five Wind Speed (WS) Categories and Their Corresponding Beaufort Scale

Category	Wind speed interval	Beaufort scale
1	WS < 5.6 m s^{-1}	0, 1, 2, 3
2	5.6 ≤ WS < 10.8 m s^{-1}	4, 5
3	10.8 ≤ WS < 17.2 m s^{-1}	6, 7
4	17.2 ≤ WS < 24.5 m s^{-1}	8, 9
5	WS ≥ 24.5 m s^{-1}	10, 11, 12

30 years or >2 days per year, Figure 10d). The near future period exhibits the same changes but with an overall lower intensity (Figure S9).

3.4. Changes in Daily Maximum Wind Speed Distributions

A visual comparison between Figures 6e and 10b shows that the change in the 98th percentile is not equal to the change in the mean, with even different signs locally (e.g., in Norway around 25°E–70.5°N). It means that the distribution of the wind speed at some grid points does not just shift toward higher or lower values but its shape changes. Therefore, we here examine more precisely how the distribution shape changes in the future using five wind categories based on the Beaufort scale as defined in Table 2.

The top row of Figure 11 shows that the weakest winds (category 1) are most frequent over the low-altitude land regions such as southeastern Norway, Sweden, and Finland, whereas for seas, most of the days have winds in category 3. The lakes in southern Sweden have most often winds in category 2. The Norwegian and North seas experience winds in category 4 but the more sheltered Baltic Sea has less days with wind in this category. Categories 4 and 5 highlight the mountainous areas and an area over sea close to the Norwegian coast (5°E–62.5°N) known for its strong winds (see e.g., Barstad & Grønås, 2005). When splitting the percentages in seasons, we find that winter (DJF) has the largest share of strong winds over mountains and sea, especially in categories 3 and 4. The largest share of weak wind speeds (category 1) is found in summer (JJA) over the whole domain (land and sea) compared to the other seasons. Winds in category 2 are most frequent in summer over water and mountains but they are more frequent over low-altitude land in winter. Note that the wind distribution over Denmark is different than for the others low-altitude areas, such as the neighboring Sweden, as, because of its location east of the North Sea, it is much more exposed to the passing low pressure systems. It has less frequent winds in category 1 than in category 2 compared to Sweden for example, In summer, winds in category 5 are absent. They are more frequent in winter followed by spring (March-April-May, MAM) and fall (September-October-November, SON).

Over the Norwegian Sea, there is a flattening of the distribution with more days with wind in categories 1, 2, and 5 and less days with wind in categories 3 and 4 (Figure 12, top row). The increase in number of days in categories 1 and 2 occurs in all seasons (Figure 12, bottom rows), whereas it occurs mostly in fall (SON) and winter (DJF) for category 5 with a decrease in spring (MAM). It is difficult to get a general conclusion for Norway as a whole as the changes depend on the region considered. Over northern Norway, the number of days with wind in categories 3 to 5 decreases but increases in category 2 (Figure 12, top row). In category 1, there are both local increases and decreases. Over southwestern Norway, there is an increase in the number of days in categories 1 and 5 but a decrease in the other categories, also hinting at a flattening of the distribution. Over southeastern Norway, Sweden, and Finland, the largest changes are for weak winds in categories 1 and 2 which both cover most days (Figures 11 and 12, top rows). In accordance with Figures 6e and 7e, Figures S5b and S5e in Supporting Information S1, there is an increase of the wind speed with less days with weak winds in category 1 and more days with wind in category 2 when considering the whole year, winter, spring, and fall (Figure 12, 1st, 2nd, 3rd, and 5th rows). In summer, it is the other way around with a decrease of the mean wind speed (Figure 8e) associated with an increase of the number of days in category 1 and a decrease in category 2 (Figure 12, 4th row).

The near future exhibits similar changes to the far future although with weaker intensity (Figure S10). The largest difference is the strong decrease in the number of days in category 5 over the Norwegian Sea north of 62.5°N in winter and the whole year compared to the increase along the coast in the far future. In addition, for category 5, in spring (fall), there is also a different sign of the change with a slight increase (decrease) in the near future but a decrease (increase) in the far future (compare Figure 12, Figure S10).

As the strongest winds are the most interesting due to their potential impacts on nature and population, we here highlight the absolute and relative changes in the number of days in the highest wind category experienced during the historical period at each grid point (Figure 13a). In agreement with Figure 11, the highest wind category decreases when going east over land, from category 5 over Norway to category 2 in some places in Finland. The seas and Denmark have the highest wind in categories 4 or 5. The pattern of the far future changes in the highest wind category at individual grid points (Figures 13b and 13c) is very similar to the pattern of the change in the 98th percentile (Figures 10b and 10d). Overall over Scandinavia, there is an increase in the number of days in the highest wind category with only local negative changes mainly in central and northern Norway (Figures 13b and 13c).

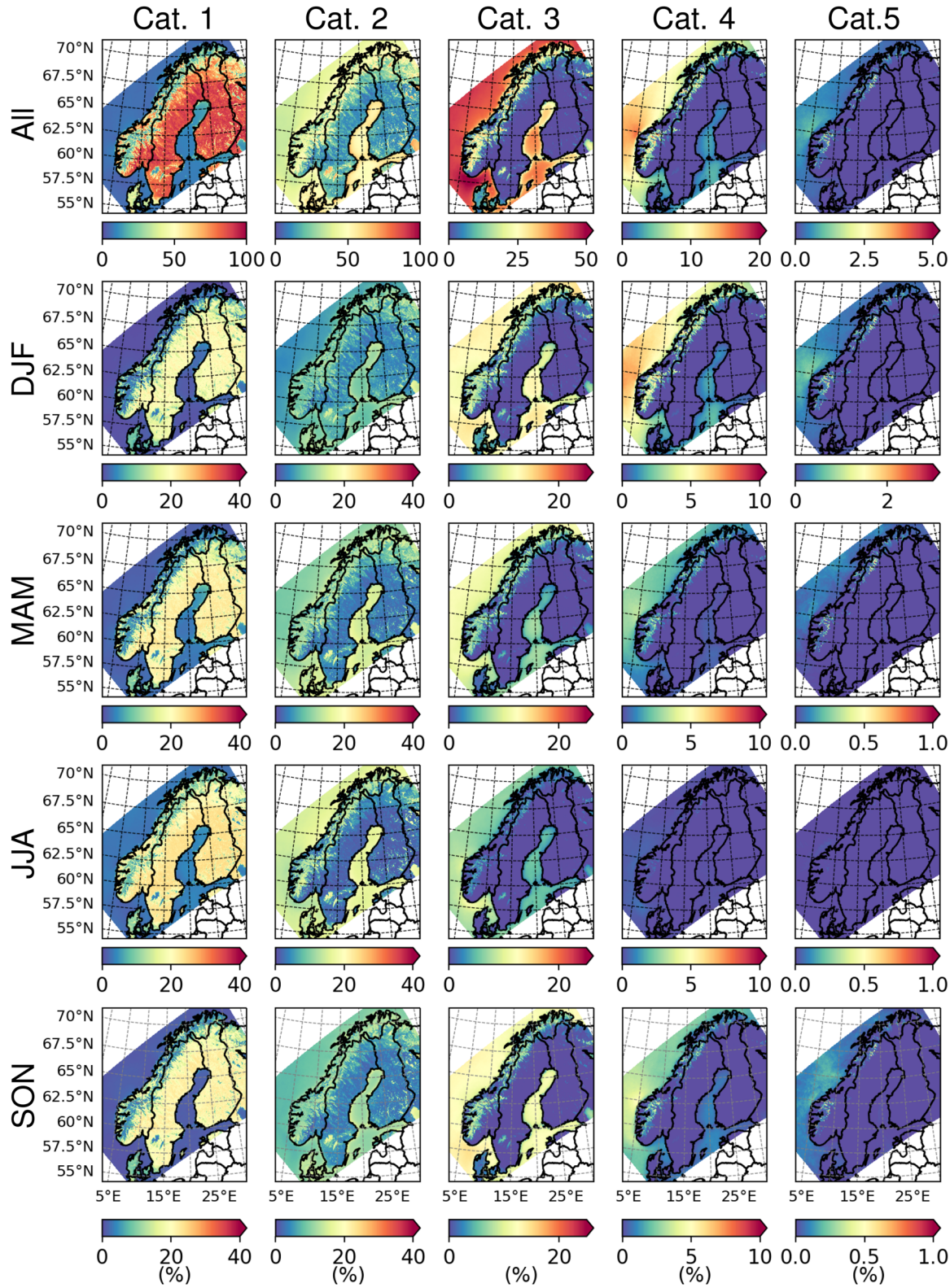

Figure 11. Percentages of days in each wind category for the whole period 1985–2014 (top) and each season (bottom). The percentages are calculated against the total number of days in the whole period using the bias-corrected wind speeds. Note the different colorbars for the top row, for December-January-February, and the three other seasons (March-April-May, June-July-August, and September-October-November).

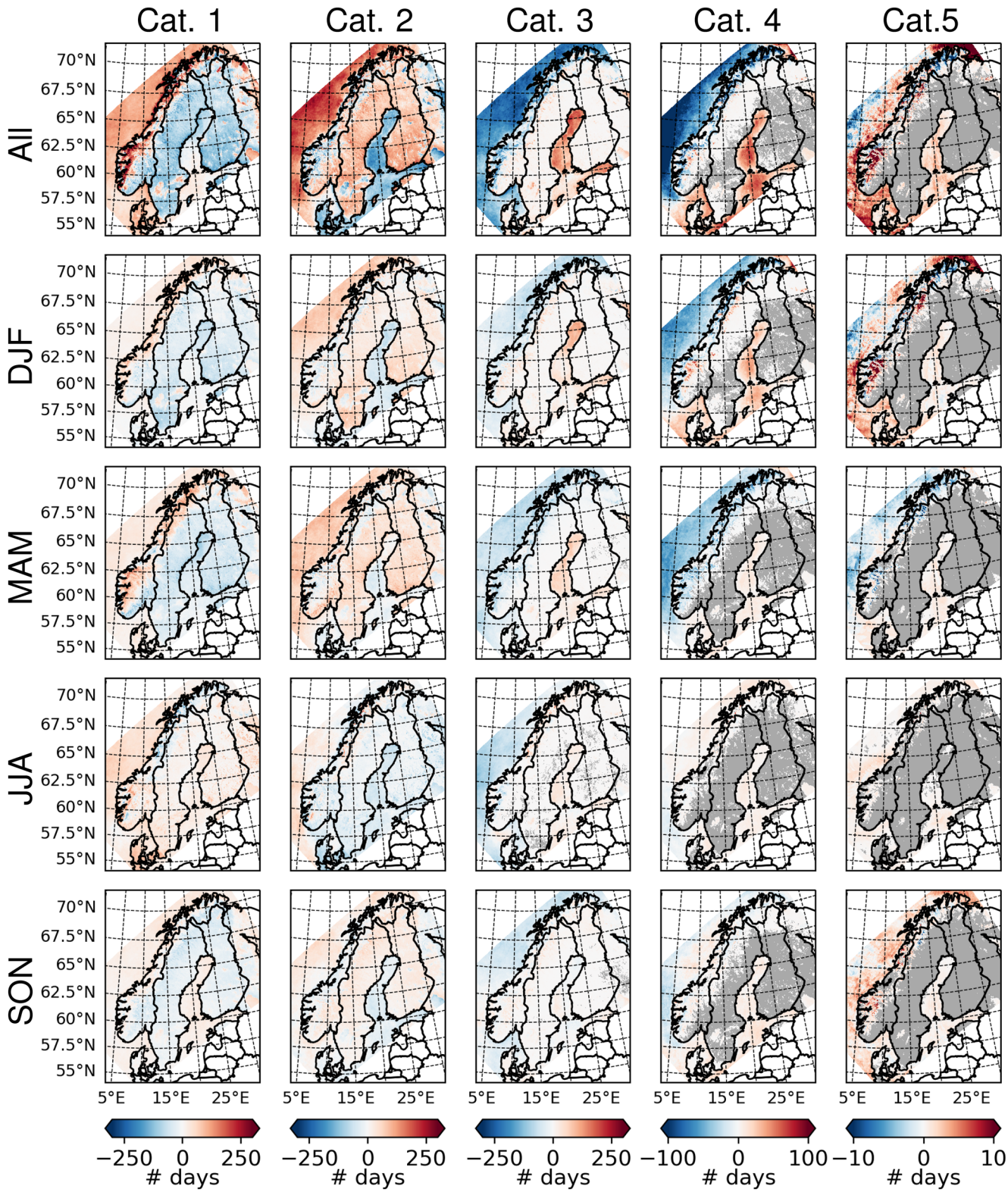

Figure 12. Far future change in the number of days over 30 years in each wind speed category for (top row) the whole year and (bottom rows) the four seasons (December-January-February, March-April-May, June-July-August, and September-October-November) using the bias-corrected wind speeds. The gray shading means that there is no day in the category in both present and future periods.

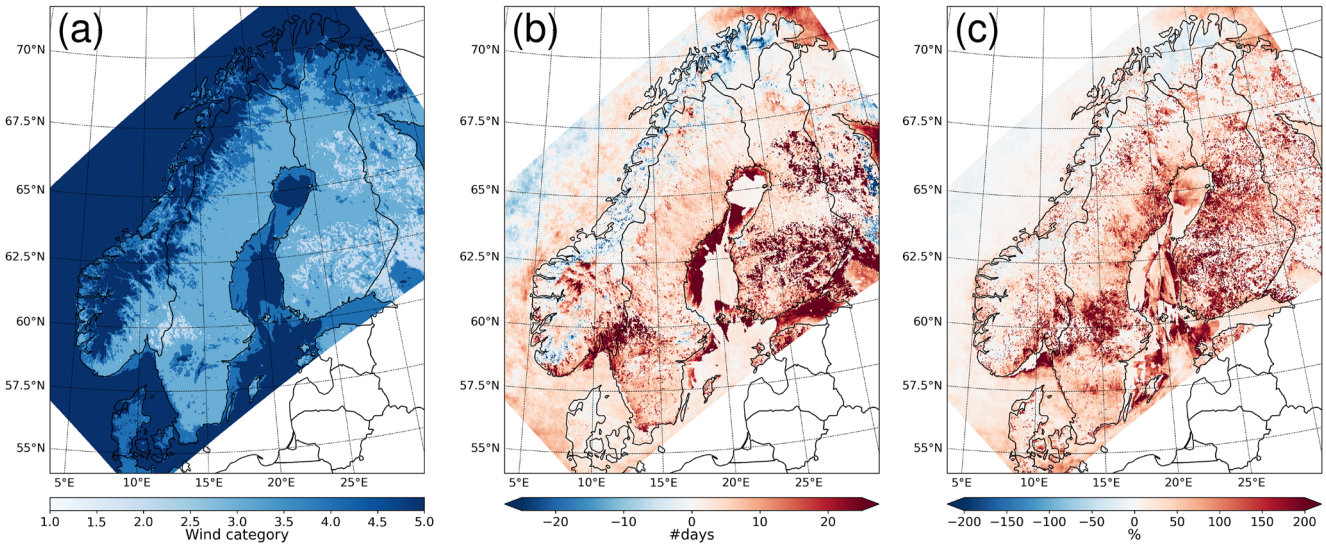

Figure 13. (a) Highest wind category containing at least 1 day with wind in this category considering the whole historical period bias-corrected wind speeds. Far future (b) absolute and (c) relative change in the number of days in the highest wind category.

3.5. Summary at Country Scale and Model Uncertainty

In order to get a more general picture of the change in the mean and 98th percentile for each country, we represent the distributions of their respective grid points (Figures 14a, 14c, 14e and 14g) and provide associated figures in Table 3. As already seen on the maps, Norway is the country with the largest spatial spread in the changes compared to the three other Scandinavian countries, namely Sweden, Finland, and Denmark, with simultaneous increases and decreases of the mean or 98th percentile of the daily maximum wind speed. For almost all countries, seasons, the mean or 98th percentile, the spatial spread, as seen from the minimum-maximum range and the IQR, increases for the far future period compared to the near future. Apart from Norway, the spatial spread is also larger in winter than in summer (compare Figures 14c and 14e).

For Norway, the spatial mean daily maximum wind speed (diamond symbol in Figure 14a) gets weaker in both future periods but this change is not very representative as only 64%–69% (for the annual mean) of the country's grid points have a negative change (see Table 3). This mean change is linked to the change in winter whereas in summer the mean change is closer to 0 (Figures 14c and 14e, Table 3). Denmark also experiences a weaker mean wind in the future, but there is only a country-scale robust change in the near future when considering all year with 98.5% of the grid points having negative values (Figure 14a, Table 3). Note that the change is not linear with time (Figures 14c and 14e, Table 3). In winter (Figure 14c, Table 3), the country-scale change is slightly negative in the near future but becomes positive in the far future. However, in summer (Figure 14e), the mean change is negative for both periods and even larger in the far future with 99.5% of the country's grid points agreeing in the sign (Table 3). Both Sweden and Finland exhibit an increase in the mean wind which is getting larger in the far future but there is a large spread within each country (Figure 14a, Table 3). In winter, the change in the near future is close to 0 but is positive in the far future (Figure 14c, Table 3). In summer, the mean change is negative and gets more negative in the far future with 89.7% and 98.9% of the grid points below 0 for Sweden and Finland, respectively (Figure 14e, Table 3). Finally, note that although Denmark is a small country, the spread among the grid points is similar to the spread for Finland, a country almost 8 times bigger.

For the 98th percentile (Figure 14g), Norway exhibits a more pronounced decrease in the near than far future but there is a large spatial spread in the change within the country. Only between 64% and 76% of the grid points have the same sign as the national mean (Table 3). Over Sweden, Finland, and Denmark, the 98th percentile increases in the near future period and even more in the far future period. Note that the spatial spread in the changes in the 98th percentile is much larger than for the mean (compare Figures 14a and 14g) which hints at a modification of the shape of the wind speeds distributions.

Figure 14 highlights the large spread among all 20 simulations in the country-scale change in the mean and 98th percentile. There is overall no clear gathering by GCM or RCM. However, for the mean change over

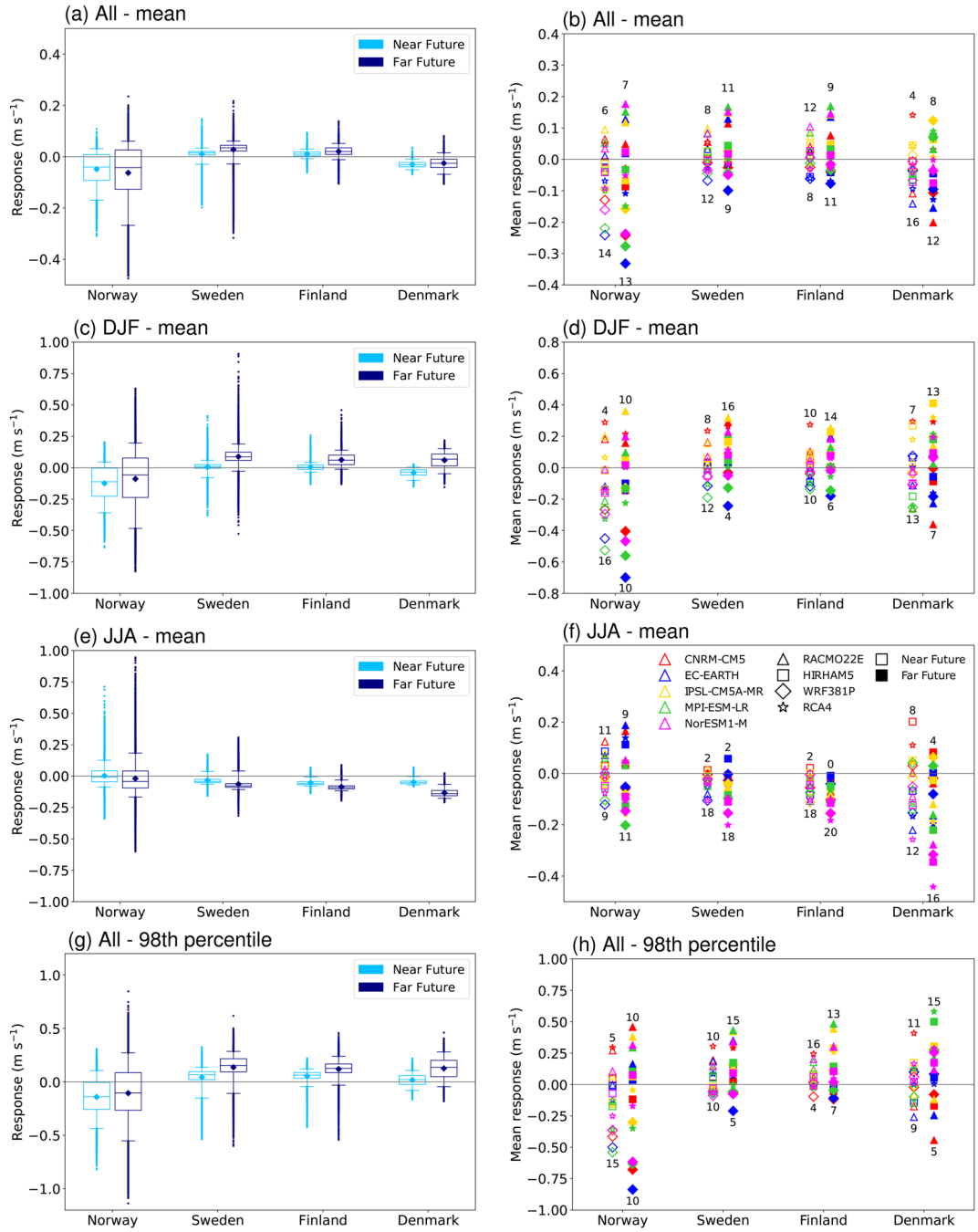

Figure 14. (a, c, e, g) Distributions of the grid point values of the multi-model mean response for (a, c, e) the daily maximum wind speed mean and (g) its 98th percentile for the four Scandinavian countries and the two future periods. Due to their different areas, the number of grid points in each country varies: Norway 36043, Sweden 49601, Finland 36826, and Denmark 4773. (b, d, f, h) Country-scale average of the simulation (b, d, f) mean and (h) 98th percentile of the daily maximum wind speed for each of the simulations. The numbers above and below each vertical line of symbols show the number of simulations above and below 0, respectively. The empty symbols represent the near future response and the filled symbols the far future period. Panels (a and b) display the response of the mean over the 30 years, while panels (c and d) and (e and f) are the responses for the winter and summer means, respectively.

Table 3
Changes in the National Averages of the Bias-Corrected (Top) Mean Daily Maximum Wind Speed for All Years (ANN), Winter (December-January-February (DJF)) and Summer (June-July-August (JJA)) (in m s^{-1}), (Middle) the 98th Percentile (in m s^{-1}), and (Bottom) the Absolute and Relative Change in the Number of Days in the Local Historical Highest Wind Category for All Years Between the Near Future (NF) and Far Future (FF) Periods and the Historical Period

		Norway		Sweden		Finland		Denmark	
		NF	FF	NF	FF	NF	FF	NF	FF
Mean (m s^{-1})	ANN	−0.05	−0.06	0.01	0.03	0.01	0.02	−0.03	−0.03
	DJF	−0.12	−0.09	0.01	0.09	0.004	0.06	−0.04	0.06
	JJA	0.003	−0.02	−0.03	−0.06	−0.05	−0.09	−0.05	−0.13
% GP	ANN	68.7	64.4	84.2	88.4	84.1	88.6	98.5	84.4
	DJF	76.8	57.2	68.3	92.9	56.1	91.1	92.2	83.2
	JJA	45.1	65.1	85.4	89.7	97.1	98.9	95.3	99.5
# sim	ANN	14	13	8	11	12	9	16	12
	DJF	16	10	8	16	10	14	13	13
	JJA	11	11	18	18	18	20	12	16
98th percentile (m s^{-1})	ANN	−0.14	−0.11	0.04	0.14	0.05	0.12	0.02	0.13
% GP	ANN	75.8	64.2	80.1	88.2	89.6	93.1	63.2	87.5
# sim	ANN	15	10	10	15	16	13	11	15
Highest wind cat. (# days)	ANN	0.65	3.51	4.06	7.05	10.80	20.52	0.93	1.86
% GP	ANN	62.5	66.1	89.8	91.8	93.1	93.9	81.4	88.8
Rel. change (%)	ANN	22.7	31.3	48.3	63.1	69.0	81.9	25.3	39.3
% GP	ANN	63.8	67.4	90.4	92.3	93.6	94.3	83.4	90.0

Note. The rows named % GP give the percentage of the countries' grid points having the same sign of the change as the mean, 98th percentile, in the number of days, and in the relative change in the number of days. The rows named # sim give the number of EURO-CORDEX simulations among the 20 considered here having the same change as the ensemble mean.

Norway (panel b), we see that all downscalings with RACMO22E exhibit a positive change and all downscalings with WRF381P a negative change (see also Figures S6 and S7 in Supporting Information S1) but it is not the case in DJF (see Figure 14d). The largest model agreement in the changes occurs in summer with a decrease in the wind speed in Sweden and Finland in 90% or 100% simulations (Table 3), in agreement with Figure 14e.

In accordance with Figure 13, the number of days in the historical highest wind category increases in every country but with a smaller intensity in the near future compared to the far future (Table 3). The changes are larger for Sweden and Finland than for Norway and Denmark, again due to the smaller agreement on the sign of the change within the country, especially Norway. The largest change occurs in Finland in the far future (Table 3) with an average increase of about 20 days (or a relative increase of ∼82%) in the category of strongest winds within the historical period, that are categories 2 and 3 (Figure 13a). These results suggest that adaptation measures to this more frequent large wind (between 5.6 and 17.2 m s^{-1} according to Table 2) may be required in Finland and in a lesser extent in Sweden in the far future if we follow the emission scenario RCP8.5.

Figure 15 shows that the simulations do not respond linearly to the warming and that there is no obvious link between the warming and the daily maximum wind speed change at country scale. The warming response seems mostly driven by the GCM whereas the wind speed response also depends on the RCM. It is clear that the GCM IPSL-CM5A-MR exhibits the largest mean warming for every country (see yellow symbols). For Norway, the WRF downscalings have the strongest negative response out of the four RCMs for both future periods (see also Figure 14). On the contrary, RACMO22E downscalings have the highest positive response out of the four RCMs for both future periods and it is also valid for Sweden and Finland.

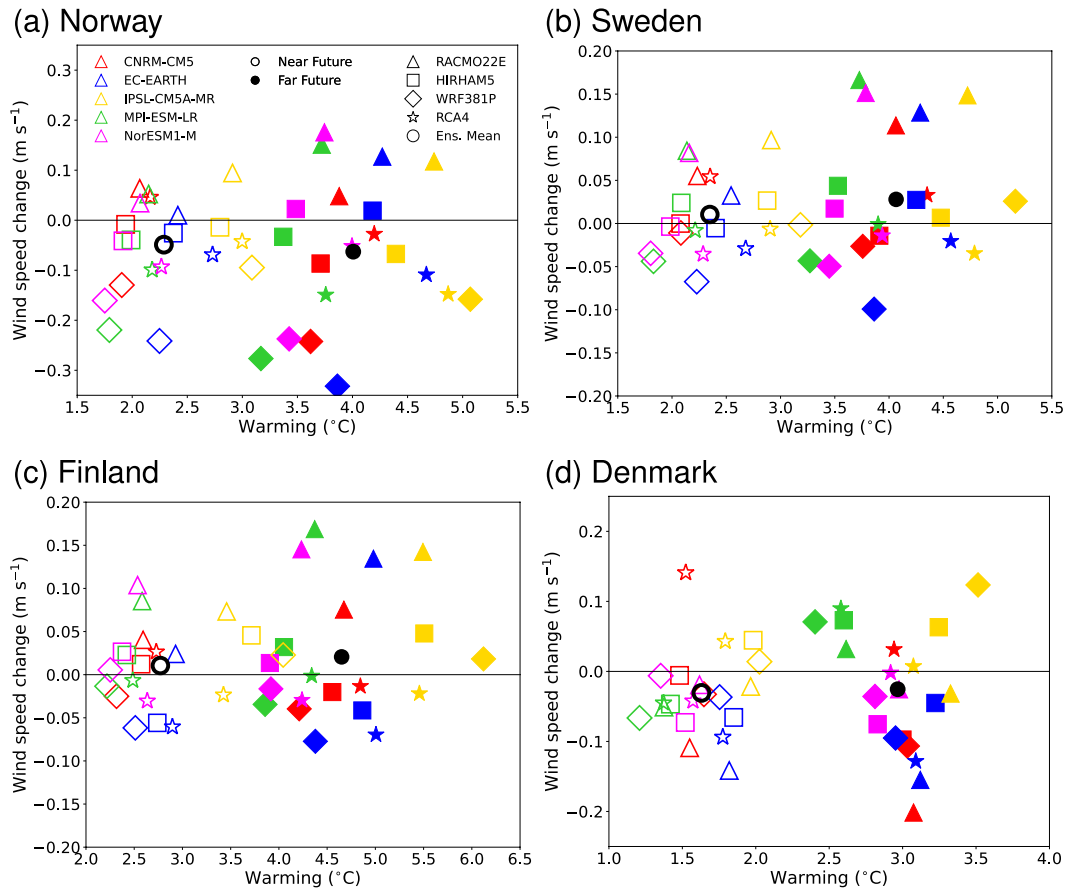

Figure 15. Country-scale average of the daily maximum wind speed change in the near future (open symbols) and far future (filled symbols) as a function of each country's mean warming for each of the 20 downscalings. Norway is shown in panel (a), Sweden in panel (b), Finland in panel (c), and Denmark in panel (d). Various colors differentiate the five global climate models and various symbols the four regional climate models. The open and filled circles show the ensemble mean for each future period. Note the different *x*- and *y*-axis in each panel and that the near-surface air temperature was not bias-corrected contrary to the wind speed.

4. Discussion

The simulations bias depend on the reference data set used for comparison, on the percentile evaluated, and also on the method to calculate the daily maximum wind speed. For example, Vautard et al. (2021) used ERA5 to estimate the bias of 55 EURO-CORDEX simulations and found opposite signs as we do, with positive bias in the median of the daily mean wind speed over Norway and negative bias over Sweden (same results for the daily maximum wind speed but not shown in their study). Moreover, they also show that weak winds (5th percentile) are underestimated compared with ERA5 over Scandinavia, except along the western coast of Norway, while strong winds (95th percentile) are overestimated. As written in Section 2, the CMIP5 GCMs and EURO-CORDEX RCMs use model timesteps to compute the daily maximum wind speed whereas the NORA3 hourly wind speed is instantaneous. Therefore, the daily maximum wind speed should be relatively accurate compared to reality in EURO-CORDEX if the GCMs and RCMs were perfect but underestimated in NORA3 because of the smaller temporal sampling. We find that RCMs RACMO22E and HIRHAM5, for example, are still negatively biased over the Norwegian mountains (Figure 4) meaning that they do not perform well in this area. However, where the bias is positive, for example, over Sweden (Figure 4), it is not clear if the issue comes from the RCM overestimating the wind or NORA3 underestimating it because of its low-frequency temporal sampling.

The changes in the raw mean winds we obtain here are in agreement with some previous studies. Christensen et al. (2022), who used the mean wind speed at 10 m of five GCMs downscaled with the same RCM, RCA4, also found the negative change along the Norwegian coast and positive change in the Baltic Sea in winter in addition

to the increase of wind speed in summer over Finland, Sweden, and southeastern Norway. They also showed the dipole with negative change over Norway and positive over Sweden around 68°N and 15°–10°E. They emphasized the lack of robustness of the wind change over most land areas, as we have also highlighted, and the influence of coupling the atmospheric RCM with an oceanic model, which can change the sign of the response over the Baltic Sea but also change the response in more remote places (see their Figure 12). Using three downscalings with two GCMs and two RCMs, Schwierz et al. (2010) also found a decrease in the wintertime mean (October to March) wind gust in northern Scandinavia and an increase over Denmark but with amplitudes larger than what we detected. In addition to the different wind variables used, the discrepancy may arise from the historical period used by Schwierz et al. (2010) starting 24 years earlier than ours (1961–1990 in their study compared to 1985–2014 in ours) and our use of a larger ensemble.

However, our results are noticeably different from the findings of Mioduszewski et al. (2018) who investigated the related future change between the atmospheric static stability and monthly mean 10-m wind speed (not the daily maximum wind speed) over the high latitudes of the Northern Hemisphere using the CESM large ensemble. In addition to the different variable used, the discrepancies with Mioduszewski et al. (2018) also probably comes from the much coarser resolution of CESM. Mioduszewski et al. (2018) found an increase in stability most of the time by the end of the 21st century over Scandinavia but with some local decreases along the Norwegian coast in summer and in Denmark, Southern Norway, southern Sweden, and southern Finland in winter. Accordingly, the wind decreases almost everywhere in the domain. However, in summer, the wind increases where the stability decreased at two locations in northern and southwestern Norway. Moreover, not all wind changes were linked to static stability as, for example, in winter in southern Sweden, where both the wind and static stability decrease.

Using the IPCC WG1 Interactive Atlas (https://interactive-atlas.ipcc.ch/regional-information), we can see that the long-term (2081–2100) multi-model mean projections of the mean surface wind speed compared to the baseline period (1981–2010) have similar patterns in the 48 EURO-CORDEX experiments (RCP8.5 scenario) and 31 CMIP6 models (SSP585 scenario). However, they can strongly differ in magnitude and sign in some regions, such as Scandinavia. For example, in winter, CMIP6 projections are negative in northern Sweden and Finland but positive in EURO-CORDEX. In summer, CMIP6 projects negative changes over Scandinavia whereas EURO-CORDEX exhibits a band of positive changes in northern Norway (as also seen in our Figure 8b). From this comparison, we do not expect very different results in the on-going new EURO-CORDEX exercise.

Future changes in the 10-m daily maximum wind speed could be due to changes in the number of cyclones in the area, but it is not that straightforward. Zappa et al. (2013) found in CMIP5 simulations, among which some GCMs were downscaled in the EURO-CORDEX exercise, a reduced number of cyclone tracks over the whole Scandinavia in summer and a reduced (increased) number in northern Scandinavia (the British Isles and North Sea) in winter. The decreased mean daily maximum wind speed we find over most of Scandinavia in summer could be associated with cyclones being less frequent. However, the summer-time increase in wind speed over northern Norway cannot be associated with a change in cyclone occurrence. In winter, the increased number of cyclone tracks in the southern part of the domain could be related to the stronger wind speed we identified in the future periods and the lack of cyclones to the northern part could be related to the weaker wind speed we show in northern Norway. However, most of the future changes in wind speed we find cannot be explained by the change in cyclone occurrence.

In winter, the increased wind in western Denmark and southern Sweden (Figure 7e) can be associated with more cyclones steered toward this area because of the acceleration of the 500-hPa jet over northern Europe/southern Scandinavia found by Ozturk et al. (2022) using monthly mean wind in 42 EURO-CORDEX simulations. Concomitantly, there is a decrease in the wind speed at 500 hPa over northern Scandinavia (see Figures 3a–3c in Ozturk et al., 2022) that can be related to the decreased wind over the sea and northern Norwegian land (Figure 7e). However, in summer, the future 500-hPa jet does not change much over Scandinavia compared to the historical period (see Figures 3i–3k in Ozturk et al., 2022), which does not explain the decrease in mean near-surface daily maximum wind speed we find over most of the domain in Figure 8e.

A comparison of our results with previous studies that investigated the future projections of the 98th percentile of the daily maximum wind speed or gust (Donat et al., 2011; Pryor et al., 2012; Schwierz et al., 2010) highlights some agreements and disagreements. The changes in the 98th percentile we find are similar to Donat et al. (2011) who showed, in some downscalings, an increase in the 98th percentile of the daily maximum wind speed (same variable as we use here) over southern Scandinavia, including southern Sweden and Denmark, by the end of the 21st century (their Figure 5b). The earlier study by Schwierz et al. (2010) found a decrease in the 98th percentile of the daily

wind gust over northern Sweden and Norway whereas we find this decrease in wind speed mainly over northern Norway only with weaker values. The increase we find over southern Denmark is also in agreement with Schwierz et al. (2010) but they do not have the north-south discrepancy in the 98th percentile change that we get although they find it in the change in the mean (compare the two first rows of their Figure 7 with our Figure 10b). Finally, Pryor et al. (2012) also found this dipole in the change of the wind gust by 2071–2100 with a decrease in northern Norway and Sweden and an increase of the wind gust in southern Sweden and Denmark but their ensemble of three members emphasizes large differences among the runs hence a large uncertainty in the results.

In agreement with Christensen et al. (2022), we find a non-robust relationship between the country-scale average warming and daily maximum wind speed change. The warming signal is mainly determined by the GCM while the wind speed change is driven by both the GCM and RCM. By discriminating the GCMs and RCMs used, we are able to show that RCMs sometimes exhibit a consistent (same sign) response independent of the GCM downscaled but that is not a general rule.

Trends in the annual and seasonal means of the NORA3 daily maximum wind speed over the period 1980–2020 (41 years) exhibit remarkable differences with the EURO-CORDEX projections. The most striking difference occurs in summer where NORA3 shows positive trends over the Norwegian Sea, southern Norway, Sweden, Finland, and Denmark whereas EURO-CORDEX shows negative responses (compare Figure S11g in Supporting Information S1 with Figure 8e). Other differences include opposite signs over the largest lake in Sweden with positive trends in all seasons but negative responses in the annual and winter means for EURO-CORDEX, the positive trend around 65°N over the Norwegian Sea and Norway contrary to the negative responses in EURO-CORDEX, and the positive trend in the Skagerrak in all seasons but negative response in EURO-CORDEX mainly in the annual and summer means (compare Figure S11 with Figures 6e, 7e and 8e and Figure S5). However, both NORA3 and EURO-CORDEX exhibit negative trend and response in northern Norway and positive trend and response over the Gulf of Bothnia in the annual and winter means. These agreements and differences call for deeper investigations. Finally, one can notice the high uncertainty of the mean wind speed trends (Figures S11b, S11d, S11f, S11h and S11j) due to the high interannual variability (not shown).

5. Conclusion

In this study, we have investigated the changes in daily maximum wind speed over Scandinavia in two future periods (2041–2070 and 2071–2100) following the RCP8.5 scenario compared to the historical period (1985–2014) using 20 raw and bias-corrected regional downscalings among the EURO-CORDEX simulations available. We use the quantile mapping method to fit the RCM wind speed distributions to the new high resolution NORA3 hindcast, which has proven to have good skills in representing wind speed over complex topography (Haakenstad et al., 2021).

The skill of the historical 12-km resolution EURO-CORDEX simulations compared to the reference data set NORA3 is driven by the choice of the RCM and to a much lesser extent by the choice of the GCM. Most RCMs underestimate the mean daily maximum wind speed over the mountains and overestimate it over low-altitude lands of Norway, Sweden, and Finland compared to NORA3. The biases in the mean daily maximum wind speed of the 20 downscalings mostly differ over the mountains, where the largest spread is found. A decomposition of the variance of the biases shows that it is mostly associated with the RCM over land and the Baltic Sea, the GCM being most important over the Norwegian and Barents seas. However, this result can be modified depending on the set of downscalings considered. The downscalings closest to the reference data set are performed with HIRHAM5 followed by the ones made with RCA4.

In the historical period (1985–2014), the mean daily maximum wind speed is largest over the mountains, seas, and lakes especially in winter. This is due to the low roughness of the seas and lakes and the mountains exposure to passing low-pressure systems, most frequent in winter. Over the low-altitude lands of southeastern Norway, Sweden, and Finland, the mean daily maximum wind speed is largest in summer.

In the far future (2071–2100) winter, there is a decrease in the mean daily maximum wind speed over the Norwegian Sea and along the western coast of Norway sometimes larger than 0.4 m s^{-1} compared to the historical period. Elsewhere, there is an increase in the mean daily maximum wind speed, especially in southern Sweden and the Gulf of Bothnia. In summer, the mean daily maximum wind speed decreases over the Norwegian Sea, southern Norway, Denmark, and Sweden and increases over central and northern Norway as well as over the Baltic Sea. However, in agreement with previous studies (Christensen et al., 2022; Schwierz et al., 2010), we find

that the changes in the wind speed are not very robust. Because of the conservation of the relative changes during the bias correction process of the future simulations, the absolute changes are not supposed to be conserved. However, as in Ngai et al. (2022) who studied precipitation over Southeast Asia with a raw and bias corrected CORDEX ensemble, we find that the bias correction does not influence the pattern of the future changes but it modifies their amplitude, which is important for decision makers when wind thresholds are involved.

Taking the historical 98th percentile as a measure for strong winds, we find that the number of days above this threshold will increase in the future mainly over the Norwegian southeastern coast, southern Sweden, and Finland but decrease in northern Norway. Over southern Sweden, where the historical 98th percentile is relatively weak (<10 m s^{-1}), considering that these strong winds happen about 7 days every year, an increase of 2 days with those winds is not negligible and might be felt by the inhabitants.

Looking at the daily maximum wind speed distributions, the change in the far future of the distribution's shape depends on the region considered. For example, in the Norwegian Sea along the coast, the distribution seems to get flatter, with more frequent very low and very high winds, whereas over Sweden and Finland, the distribution seems to get more skewed with less frequent low-wind days.

The country-scale distributions as well as the maps of the changes in wind speed highlight that for decision-making, one needs to look at the changes in particular regions, not necessarily the administrative counties, especially for Norway where the landscape and exposure vary greatly within the country. Moreover, the daily maximum wind speed future projections for each of the four Scandinavian countries are rather independent from the warming.

Changes in cyclones frequency, 500-hPa jet, and atmospheric static stability can help justify some future increases or decreases in daily maximum wind speed over Scandinavia but not everywhere. Therefore, there is a need to investigate the processes creating wind at the local scale for the present climate and examine how these processes will be modified due to climate warming. Another future work would be the use of the bias corrected data in windstorm losses assessments knowing that the changes in wind are subject to a lot of uncertainty. Moreover, it would be interesting to evaluate the downscalings of the on-going new EURO-CORDEX exercise with updated and new RCMs. Finally, along with previous studies, it is clear that the wind speed future projections suffer from a large uncertainty. The internal variability, as shown by Pryor et al. (2012) (see their Figure 6), seems to be a source of uncertainty as well as the model uncertainty as seen for example, in our Figures 14b, 14d, 14f and 14h. Creating large ensembles of regional simulations either by downscaling large ensembles of global climate simulations, such as the ones part of the Single Model Initial-condition Large Ensemble initiative (Deser et al., 2020), or by varying the RCM physics parameters (see the 12-member ensemble of Tucker et al. (2022)) could help in distinguishing and quantifying the sources of uncertainty (Deser, 2020; Mankin et al., 2020).

Acknowledgments
C. Michel was funded by the Research Council of Norway through the project StormRisk nr 300608 granted to A. Sorteberg. The authors are grateful to the Norwegian Meteorological Institute for creating and publishing the NORA3 hindcast. The authors acknowledge the World Climate Research Programme's Working Group on Regional Climate, and the Working Group on Coupled Modeling, former coordinating body of CORDEX and responsible panel for CMIP5. The authors also thank the climate modeling groups (listed in Table 1 of this paper) for producing and making available their model output. Finally, the authors acknowledge the Earth System Grid Federation infrastructure an international effort led by the U.S. Department of Energy's Program for Climate Model Diagnosis and Intercomparison, the European Network for Earth System Modeling and other partners in the Global Organization for Earth System Science Portals (GO-ESSP).

Data Availability Statement

The EURO-CORDEX and CMIP5 data were downloaded from the Earth System Grid Federation portal https://esgf-data.dkrz.de/. The NORA3 hindcast is made publicly available by the Norwegian Meteorological Institute at https://thredds.met.no/thredds/catalog/nora3/catalog.html.

References

Abatzoglou, J. T. (2013). Development of gridded surface meteorological data for ecological applications and modelling. *International Journal of Climatology*, *33*(1), 121–131. https://doi.org/10.1002/joc.3413

Amengual, A., Homar, V., Romero, R., Alonso, S., & Ramis, C. (2012). A statistical adjustment of regional climate model outputs to local scales: Application to Platja de Palma, Spain. *Journal of Climate*, *25*(3), 939–957. https://doi.org/10.1175/JCLI-D-10-05024.1

Barstad, I., & Grønås, S. (2005). Southwesterly flows over southern Norway–mesoscale sensitivity to large-scale wind direction and speed. *Tellus*, *57A*(2), 136–152. https://doi.org/10.3402/tellusa.v57i2.14627

Barstad, I., Sorteberg, A., & dos-Santos Mesquita, M. (2012). Present and future offshore wind power potential in northern Europe based on downscaled global climate runs with adjusted SST and sea ice cover. *Renewable Energy*, *44*, 398–405. https://doi.org/10.1016/j.renene.2012.02.008

Brinckmann, S., Krähenmann, S., & Bissolli, P. (2016). High-resolution daily gridded data sets of air temperature and wind speed for Europe. *Earth System Science Data*, *8*(2), 491–516. https://doi.org/10.5194/essd-8-491-2016

Cannon, A. J., Sobie, S. R., & Murdock, T. Q. (2015). Bias correction of GCM precipitation by quantile mapping: How well do methods preserve changes in quantiles and extremes? *Journal of Climate*, *28*(17), 6938–6959. https://doi.org/10.1175/JCLI-D-14-00754.1

Chen, J., Brissette, F. P., & Caya, D. (2020). Remaining error sources in bias-corrected climate model outputs. *Climatic Change*, *162*(2), 563–582. https://doi.org/10.1007/s10584-020-02744-z

Cheynet, E., Liu, S., Ong, M. C., Jakobsen, J. B., Snæbjörnsson, J., & Gatin, I. (2020). The influence of terrain on the mean wind flow characteristics in a fjord. *Journal of Wind Engineering and Industrial Aerodynamics*, *205*, 10331. https://doi.org/10.1016/j.jweia.2020.104331

Cheynet, E., Solbrekke, I. M., Diezel, J. M., & Reuder, J. (2022). A one-year comparison of new wind atlases over the North Sea. *Journal of Physics: Conference Series*, *2362*(1), 012009. https://doi.org/10.1088/1742-6596/2362/1/012009

Christensen, O. B., Kjellström, E., Dieterich, C., Gröger, M., & Meier, H. E. M. (2022). Atmospheric regional climate for the Baltic Sea region until 2100. *Earth System Dynamics*, *13*(1), 133–157. https://doi.org/10.5194/esd-13-133-2022

Coppin, P., Bradley, E., & Finnigan, J. (1994). Measurements of flow over an elongated ridge and its thermal stability dependence: The mean field. *Boundary-Layer Meteorology*, *69*(1–2), 173–199. https://doi.org/10.1007/BF00713302

Cornes, R., van der Schrier, G., van den Besselaar, E., & Jones, P. (2018). An ensemble version of the E-OBS temperature and precipitation datasets. *Journal of Geophysical Research: Atmospheres*, *123*(17), 9391–9409. https://doi.org/10.1029/2017JD028200

Déqué, M., Rowell, D. P., Lüthi, D., Giorgi, F., Christensen, J. H., Rockel, B., et al. (2007). An intercomparison of regional climate simulations for Europe: Assessing uncertainties in model projections. *Climatic Change*, *81*(S1), 53–70. https://doi.org/10.1007/s10584-006-9228-x

Desai, A. R., Austin, J. A., Bennington, V., & McKinley, G. A. (2009). Stronger winds over a large lake in response to weakening air-to-lake temperature gradient. *Nature Geoscience*, *2*(12), 855–858. https://doi.org/10.1038/ngeo693

Deser, C. (2020). Certain uncertainty: The role of internal climate variability in projections of regional climate change and risk management. *Earth's Future*, *8*(12), e2020EF001854. https://doi.org/10.1029/2020EF001854

Deser, C., Lehner, F., Rodgers, K. B., Ault, T., Delworth, T. L., DiNezio, P. N., et al. (2020). Insights from Earth system model initial-condition large ensembles and future prospects. *Nature Climate Change*, *10*(4), 277–286. https://doi.org/10.1038/s41558-020-0731-2

Dolores-Tesillos, E., Teubler, F., & Pfahl, S. (2022). Future changes in North Atlantic winter cyclones in CESM-LE – Part 1: Cyclone intensity, potential vorticity anomalies, and horizontal wind speed. *Weather and Climate Dynamics*, *3*(2), 429–448. https://doi.org/10.5194/wcd-3-429-2022

Donat, M. G., Leckebusch, G. C., Wild, S., & Ulbrich, U. (2011). Future changes in European winter storms losses and extreme wind speeds inferred from GCM and RCM multi-model simulations. *Natural Hazards and Earth System Sciences*, *11*(5), 1351–1370. https://doi.org/10.5194/nhess-11-1351-2011

François, B., Vrac, M., Cannon, A. J., Robin, Y., & Allard, D. (2020). Multivariate bias corrections of climate simulations: Which benefits for which losses? *Earth System Dynamics*, *11*(2), 537–562. https://doi.org/10.5194/esd-11-537-2020

Haakenstad, H., Breivik, Ø., Furevik, B. R., Reistad, M., Bohlinger, P., & Aarnes, O. J. (2021). NORA3: A nonhydrostatic high-resolution hindcast of the North Sea, the Norwegian Sea, and the Barents Sea. *Journal of Applied Meteorology and Climatology*, *60*(10), 1443–1464. https://doi.org/10.1175/JAMC-D-21-0029.1

Haugen, J. E., & Iversen, T. (2008). Response in extremes of daily precipitation and wind from a downscaled multi-model ensemble of anthropogenic global climate change scenarios. *Tellus*, *60A*(3), 411–426. https://doi.org/10.1111/j.1600-0870.2008.00315x

Hemer, M. A., McInnes, K. L., & Ranasinghe, R. (2012). Climate and variability bias adjustment of climate model-derived winds for a southeast Australian dynamical wave model. *Ocean Dynamics*, *62*(1), 87–104. https://doi.org/10.1007/s10236-011-0486-4

Hempel, S., Frieler, K., Warszawski, L., Schewe, J., & Piontek, F. (2013). A trend-preserving bias correction – The ISI-MIP approach. *Earth System Dynamics*, *4*(2), 219–236. https://doi.org/10.5194/esd-4-219-2013

Hersbach, H., Bell, B., Berrisford, P., Hirahara, S., Horányi, A., Muñoz-Sabater, J., et al. (2020). The ERA5 global reanalysis. *Quarterly Journal of the Royal Meteorological Society*, *146*(730), 1999–2049. https://doi.org/10.1002/qj.3803

Hewson, T. D., & Neu, U. (2015). Cyclones, windstorms and the IMILAST project. *Tellus*, *67A*(1), 27128. https://doi.org/10.3402/tellusa.v67.27128

Jacob, D., Petersen, J., Eggert, B., Alias, A., Christensen, O. B., Bouwer, L. M., et al. (2014). EURO-CORDEX: New high-resolution climate change projections for European impact research. *Regional Environmental Change*, *14*(2), 563–578. https://doi.org/10.1007/s10113-013-0499-2

Jing-Jing, X., Fei, H., Zi-Niu, X., & Xue-Ling, C. (2014). Bias correction in wind direction forecasting using the circular-circular regression method. *Atmospheric and Oceanic Science Letters*, *7*(2), 87–91. https://doi.org/10.3878/j.issn.1674-2834.13.0057

Kunz, M., Mohr, S., Rauthe, M., Lux, R., & Kottmeier, C. (2010). Assessment of extreme wind speeds from Regional Climate Models – Part 1: Estimation of return values and their evaluation. *Natural Hazards and Earth System Sciences*, *10*(4), 907–922. https://doi.org/10.5194/nhess-10-907-2010

Lange, S. (2019). Trend-preserving bias adjustment and statistical downscaling with ISIMIP3BASD (v1.0). *Geoscientific Model Development*, *12*(7), 3055–3070. https://doi.org/10.5194/gmd-12-3055-2019

Laurila, T. K., Sinclair, V. A., & Gregow, H. (2020). Climatology, variability, and trends in near-surface wind speeds over the North Atlantic and Europe during 1979–2018 based on ERA5. *International Journal of Climatology*, *41*(4), 2253–2278. https://doi.org/10.1002/joc.6957

Lawrence, D. (2020). Uncertainty introduced by flood frequency analysis in projections for changes in flood magnitudes under a future climate in Norway. *Journal of Hydrology: Regional Studies*, *28*, 100675. https://doi.org/10.1016/j.ejrh.2020.100675

Li, D., Feng, J., Dosio, A., Qi, J., Xu, Z., & Yin, B. (2020). Historical evaluation and future projections of 100-m wind energy potentials over CORDEX-East Asia. *Journal of Geophysical Research: Atmospheres*, *125*(15), e2020JD032874. https://doi.org/10.1029/2020JD032874

Li, D., Feng, J., Xu, Z., Yin, B., Shi, H., & Qi, J. (2019). Statistical bias correction for simulated wind speeds over CORDEX-East Asia. *Earth and Space Science*, *6*(2), 200–211. https://doi.org/10.1029/2018EA000493

Mankin, J. S., Lehner, F., Coats, S., & McKinnon, K. A. (2020). The value of initial condition large ensembles to robust adaptation decision-making. *Earth's Future*, *8*(10), e2012EF001610. https://doi.org/10.1029/2020EF001610

Maraun, D. (2013). Bias correction, quantile mapping, and downscaling: Revisiting the inflation issue. *Journal of Climate*, *26*(6), 2137–2143. https://doi.org/10.1175/JCLI-D-12-00821.1

Markowski, P., & Richardson, Y. (2010). *Mesoscale meteorology in midlatitudes*. John Wiley & Sons, Ltd. https://doi.org/10.1002/9780470682104

McInnes, K. L., Erwin, T. A., & Bathols, J. M. (2011). Global Climate Model projected changes in 10 m wind speed and direction due to anthropogenic climate change. *Atmospheric Science Letters*, *12*(4), 325–333. https://doi.org/10.1002/asl.341

Mioduszewski, J., Vavrus, S., & Wang, M. (2018). Diminishing Arctic sea ice promotes stronger surface winds. *Journal of Climate*, *31*(19), 8101–8119. https://doi.org/10.1175/JCLI-D-18-0109.1

Moemken, J., Reyers, M., Feldmann, H., & Pinto, J. G. (2018). Future changes of wind speed and wind energy potentials in EURO-CORDEX ensemble simulations. *Journal of Geophysical Research: Atmospheres*, *123*(12), 6373–6389. https://doi.org/10.1029/2018JD028473

Ngai, S. T., Junenga, L., Tanganga, F., Chung, J. X., Supari, S., Salimun, E., et al. (2022). Projected mean and extreme precipitation based on bias-corrected simulation outputs of CORDEX Southeast Asia. *Weather and Climate Extremes*, *37*, 100484. https://doi.org/10.1016/j.wace.2022.100484

Nikulin, G., Kjellström, E., Hansson, U., Strandberg, G., & Ullerstig, A. (2011). Evaluation and future projections of temperature, precipitation and wind extremes over Europe in and ensemble of regional climate simulations. *Tellus*, *63A*, 41–55. https://doi.org/10.1111/j.1600-0870.2010.00466.x

Outten, S., & Esau, I. (2013). Extreme winds over Europe in the ENSEMBLES regional climate models. *Atmospheric Chemistry and Physics*, *13*(10), 5163–5172. https://doi.org/10.5194/acp-13-5163-2013

Outten, S., & Sobolowski, S. (2021). Extreme wind projections over Europe from the Euro-CORDEX regional climate models. *Weather and Climate Extremes*, *33*, 100363. https://doi.org/10.1016/j.wace.2021.100363

Ozturk, T., Matte, D., & Christensen, J. H. (2022). Robustness of future atmospheric circulation changes over the EURO-CORDEX domain. *Climate Dynamics*, *59*(5–6), 1799–1814. https://doi.org/10.1007/s00382-021-06069-0

Pinto, J. G., Fröhlich, E. L., Leckebusch, G. C., & Ulbrich, U. (2007). Changing European storm loss potentials under modified climate conditions according to ensemble simulations of the ECHAM5/MPI-OM1 GCM. *Natural Hazards and Earth System Sciences*, *7*(1), 165–175. https://doi.org/10.5194/nhess-7-165-2007

Priestley, M. D., & Catto, J. L. (2022). Future changes in the extratropical storm tracks and cyclone intensity, wind speed, and structure. *Weather and Climate Dynamics*, *3*(1), 337–360. https://doi.org/10.5194/wcd-3-337-2022

Pryor, S. C., Barthelmie, R. J., Clausen, N. E., Drews, M., MacKellar, N., & Kjellström, E. (2012). Analyses of possible changes in intense and extreme wind speeds over northern Europe under climate change scenarios. *Climate Dynamics*, *38*(1–2), 189–208. https://doi.org/10.1007/s00382-010-0955-3

Rouse, W. R. (2009). High winds over Lake Superior. *Nature Geoscience*, *2*(12), 827–828. https://doi.org/10.1028/ngeo705

Schwierz, C., Köllner-Heck, P., Zenklusen Mutter, E., Bresch, D. N., Vidale, P.-L., Wild, M., & Schär, C. (2010). Modelling European winter wind storm losses in current and future climate. *Climatic Change*, *101*(3–4), 485–514. https://doi.org/10.1007/s10584-009-9712-1

Seneviratne, S., Zhang, X., Adnan, M., Badi, W., Dereczynski, C., Di Luca, A., et al. (2021). Weather and climate extreme events in a changing climate. In V. Masson-Delmotte, P. Zhai, A. Pirani, S. L. Connors, C. Péan, S. Berger, et al. (Eds.), *Climate Change 2021: The Physical Science Basis. Contribution of Working Group I to the Sixth Assessment Report of the Intergovernmental Panel on Climate Change* (pp. 1513–1766). Cambridge University Press. https://doi.org/10.1017/9781009157896.013

Seo, H., & Yang, J. (2013). Dynamical response of the Arctic atmospheric boundary layer process to uncertainties in sea-ice concentration. *Journal of Geophysical Research: Atmospheres*, *118*(22), 12383–12402. https://doi.org/10.1002/2013JD020312

Solbrekke, I. M., Sorteberg, A., & Haakenstad, H. (2021). The 3 km Norwegian reanalysis (NORA3) – A validation of offshore wind resources in the North Sea and the Norwegian Sea. *Wind Energy Science*, *6*, 1501–1519. https://doi.org/10.5194/wes-6-1501-2021

Taylor, K. E. (2001). Summarizing multiple aspects of model performance in a single diagram. *Journal of Geophysical Research*, *106*(D7), 7183–7192. https://doi.org/10.1029/2000JD900719

Tobin, I., Vautard, R., Balog, I., Bréon, F.-M., Jerez, S., Ruti, P., et al. (2015). Assessing climate change impacts on European wind energy from ENSEMBLES high-resolution climate projections. *Climatic Change*, *128*(1–2), 99–112. https://doi.org/10.1007/s10584-014-1291-0

Tong, Y., Gao, X., Han, Z., Xu, Y., Xu, Y., & Giorgi, F. (2021). Bias correction of temperature and precipitation over China for RCM simulations using the QM and QDM methods. *Climate Dynamics*, *57*(5–6), 1425–1443. https://doi.org/10.1007/s00382-020-05447-4

Tucker, S. O., Kendon, E. J., Bellouin, N., Buonomo, E., Johnson, B., & Murphy, J. M. (2022). Evaluation of a new 12 km regional perturbed parameter ensemble over Europe. *Climate Dynamics*, *58*(3–4), 879–903. https://doi.org/10.1007/s00382-021-05941-3

Vautard, R., Kadygrov, N., Iles, C., Boberg, F., Buonomo, E., Bülow, K., et al. (2021). Evaluation of the large EURO-CORDEX regional climate model ensemble. *Journal of Geophysical Research: Atmospheres*, *126*(17), e2019JD032344. https://doi.org/10.1029/2019JD032344

Xu, Y. (2019). Estimates of changes in surface wind and temperature extremes in southwestern Norway using dynamical downscaling method under future climate. *Weather and Climate Extremes*, *26*, 100234. https://doi.org/10.1016/j.wace.2019.100234

Zappa, G., Shaffrey, L. C., Hodges, K. I., Sansom, P. G., & Stephenson, D. B. (2013). A multimodel assessment of future projections of North Atlantic and European extratropical cyclones in the CMIP5 climate models. *Journal of Climate*, *26*(16), 5846–5862. https://doi.org/10.1175/JCLI-D-12-00573.1